Design and Manufacturing Analysis of Resonantly Coupled Circuits and Other Components used for Wireless Benefit-Denial System

by

Tianyu Zhu

B.S. Mechanical Engineering
Cornell University, 2012

Submitted to the Department of Mechanical Engineering in partial fulfillment of the requirements for the degree of

MASTER OF ENGINEERING IN MANUFACTURING
AT THE
MASSACHUSETTS INSTITUTE OF TECHNOLOGY

September 2013

Signature of Author: .....

Tianyu Zhu
Department of Mechanical Engineering
August 15, 2013

Certified By: .....

Prof. David E. Hardt
Ralph E. and Eloise F. Cross Professor of Mechanical Engineering
Thesis Supervisor

Accepted By: .....

Chairman, Committee for Graduate Students
Department of Mechanical Engineering

Design and Manufacturing Analysis of Resonantly Coupled Circuits and Other Components used for Wireless Benefit-Denial System

by

Tianyu Zhu

Submitted to the Department of Mechanical Engineering
on August 15, 2013 in partial fulfillment of the requirements for the
Degree of Masters of Engineering in Manufacturing

Abstract

A new benefit-denial system using RFID technology and inductive heating is under development by ProTeqt Technologies. During the deactivation process, an enabler receives electromagnetic waves and turns the energy to heat, causing the polymeric material inside to expand and create force. An LC circuit in the locking mechanism, acting as a weakly coupled electromagnetic resonator, is used to improve energy transfer efficiency. The design of the LC circuit, as well as the measurement of the resulting force is presented. Due to the manufacturing variability of each component, the force generated by the enabler in the lock is uncertain. In the thesis, an analysis of the manufacturing variability and the distribution of the resulting force was conducted. A simulation model was developed to predict the robustness of the lock system. The test results show that the force generated is significantly more than the force needed, proving that the unlocking process is highly reliable. The result generated by the simulation validates the force test results.

Thesis Supervisor: David E. Hardt
Title: Professor of Mechanical Engineering

For my grandmother,

Meibao Shen

Acknowledgements

First of all, I would like to thank MIT and ProTeqt Technologies for providing us with this excellent internship opportunity. Without the support from both ends, this project would not have had a good start.

David Hardt, the head of my program and my thesis advisor, was always there to help us overcome obstacles in the way of our project. When we were unclear about the future direction of the project, his recommendation opened new doors for us.

Many thanks need to go to Dan Bean, senior mechanical engineer at ProTeqt. Being the person who worked the most closely with us during the internship, he was extremely supportive, giving us the insight and resources needed to carry the project forward.

George Raniuk, one of the shareholders of the company, generously shared with us his venture experience in Singapore managing world-class manufacturing plant, and his insight of start-ups.

My greatest appreciation has to go to my excellent teammates: Mitch Krogman and Amaury Rony. Coming from diverse backgrounds, they brought new perspectives, fresh ideas and different strength. Yet, we still managed to work efficiently as a team. It was a truly rewarding experience for me as I learned so much from my wonderful teammates.

I would like to thank Jennifer Craig for giving me advice regarding the writing of this thesis. Thanks to Jose Pacheco for managing the logistic of the MEngM program.

Last but not least, I want to thank my family for their unconditional support, not only on this project but also throughout my life. My parents have made a huge sacrifice to help me pursue my degree in the US. Their advice and support has always been the backbone of my achievement.

Table of Contents

List of Figure

List of Table

1 Introduction

1.1 General Research Topic

The foundation of this thesis is centered on ProTeqt Technologies, a company dedicated to providing anti-theft devices (known as "benefit denial solutions") for the electronics retail industry. In particular, we are developing a technique that can be used to expand their product functionality, based upon a mechanical locking mechanism for a Micro USB port. More explicitly, we are developing components and understanding parameters that will increase the distance from a disabling device that their technology can be used by extending a magnetic field via resonant coupling and understanding the interactions within their product.

1.2 Need for Benefit Denial Solutions against Retail Theft

Global retail theft has increased dramatically in recent years, driven by the expansion of online marketplaces [1]. Large online market places such as eBay have given rise to organized retail theft. These online markets make buying and selling stolen items easier than ever. Despite huge investments from retailers and manufacturers (more than $28 billion in 2011 [2]), this plague has continued to grow steadily. The most common solution to prevent theft in retail stores is an electronic article surveillance (EAS) system that will alert a retailer if a product passes through the doors prior to purchase. EAS systems have the limitation that the retailer still has to respond to the alert, and this response is often hesitant. In some cases, retailers explicitly tell their employees not to confront those suspected of theft. Increased shrinkage, coupled with non-effective EAS systems, has lead retailers to restrict consumer access for high-theft products (e.g. locking glass or back room cages). It is estimated that these actions reduce sales by at least 25% [2]. Moreover, these solutions attempt to address theft only at the point of sale. They fail to address the largest component of shrinkage in the retail industry: organized theft throughout the supply chain (53% of theft in North America [2]).

As the result, retailers are looking for solutions that will provide more security than the current theft prevention methods. They are interested in eliminating the motivation to steal: the resale or use of the product. ProTeqt Technologies has addressed this solution by developing a new type of mechanical lock system that temporarily disables the product, rendering it unusable until it is legally purchased. At the point-of-sale, a deactivating tablet recognizes the product using a RFID tag embedded in the packaging. It then emits a certain electromagnetic signal, based on the product, that deactivates the mechanical lock. If the product is stolen, the lock cannot be removed without damaging the product. Furthermore, their solution can also be easily integrated with current EAS systems using the existing RFID tag.

1.3 Product Components and Performance

ProTeqt's system is comprised of three key components: the deactivation tablet, cloud database and mechanical lock. The research covered by this thesis focuses on two of the three elements: the deactivation tablet and the mechanical lock. However, to fully understand ProTeqt's technology and the sequence of events that takes place, we must briefly consider all three components.

At the point of sale, the sales clerk first scans the product containing ProTeqt's lock. The RFID is then recognized, allowing the system to look up data corresponding to that particular product in the ProTeqt database. If the product has not previously been unlocked, a certain frequency is gathered from the cloud database that coincides with the product at hand. The clerk then positions the product in such a way that the lock is directly over the center of the tablet. With the product in position, the tablet creates a strong electromagnetic field at the appropriate frequency to deactivate the mechanical lock. The customer takes the product home, and uses his or her product as if the lock was never there. They are able to simply remove the lock and throw it away.

1.3.1 Deactivation Tablet

The deactivation tablet is a highly integrated computer system. It uses RFID detection to recognize products, an Internet connection to access the cloud database, LED lights to

guide the product to the center of the tablet, a function generator to produce certain frequencies, and finally a large coil to generate an electromagnetic field. The tablet must be small and unobtrusive to provide easy integration at the point of sale.

ProTeqt has contracted the design and manufacturing of the deactivation tablet to MACK Technologies[1], whose expertise is in circuit board and complex system assembly. While we may not be designing or analyzing the system for manufacturability, we need to understand the full functionality and design parameters of the deactivation tablet to further understand the effects it has on other components like the mechanical lock.

1.3.2 Mechanical Lock

The mechanical lock is a small device that is added to a consumer product at the manufacturing site. The lock is designed to eliminate key features of a product. By encapsulating and interacting with the consumer product, both internally and externally, the device is completely protected from use if it's not legally purchased.

The lock design is highly dependent on key product features that can be used to render the product unusable. At the time of this project, locks have been designed for two product lines: USB thumb drives and CD-type disks (Figure 1). For the USB thumb drives, the lock is attached to the male plug. An improper attempt to remove the lock will permanently damage the plug, rendering the thumb drive useless. For the disks, the lock secures the disk to its case. Improper removal will break the disk or the packaging.

[1] 27 Carlisle Road, Westford, MA 01886

Figure 1 The thumb drive lock (Left) and the CD-disk lock (right). Locking mechanisms are identified by the pad-lock symbol.

For this project, all the work was focused on a newly developed micro-USB lock (Figure 2). It contains a spring, two sheet metal pieces, a plastic component, an enabler, and an LC circuit. The optimized LC circuit with the enabler sitting directly on top is shown in the lower portion. Above the LC circuit is a plastic component that is forced upward by the expanding enabler. The plastic component engages the sheet metal 1. The lock is attached to the micro-USB port through the teeth of the sheet metal 1 (right end of the sheet metal 2). The entire locking system relies on the contact surfaces between sheet metal 1 and 2, especially the vertical frictional contact surface between these two components (hidden by the left end of metal sheet 2) that latches the two sheet metal pieces.

The enabler is the component in the lock that expands when inductively heated. The whole system depends on the enabler expanding enough to fire the unlatching device when it receives energy from the deactivation tablet. The enabler consists of a polymeric material that is sandwiched between two sheets of metal foil. At deactivation, the metal foil on the enabler intersects with lines of flux produced by the deactivation tablet. These lines of flux generate eddy currents that inherently produce heat. When the parameters are correct, this heat forces the polymeric material in the enabler to expand, exerting a force on the other components in the lock.

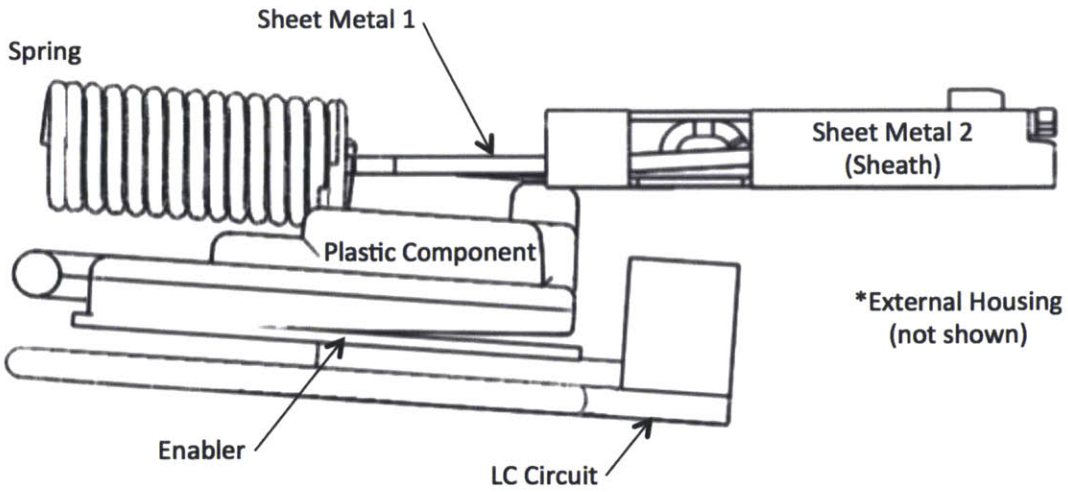

Figure 2 Internal diagram of the micro-USB lock, developed by ProTeqt

When the enabler expands, the plastic component is pushed up and bends the sheet metal 1. Thus, sheet metal 1 and 2 lose their vertical contact surface (Figure 3). The spring pushes the sheet metal 1 horizontally through the sheath (sheet metal 2). This displacement releases the teeth from the micro-USB port.

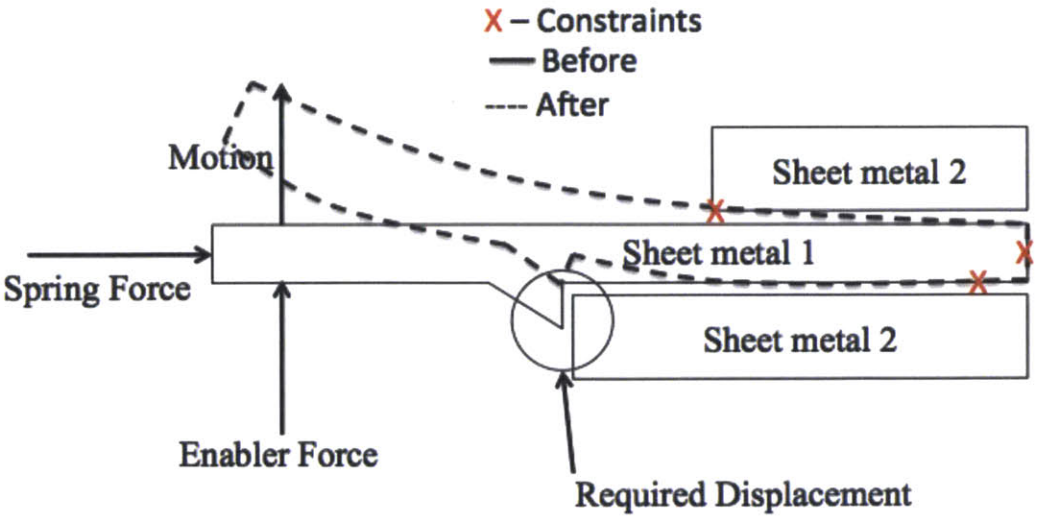

Figure 3 Schematic diagram of the sheet metal movement during deactivation

1.3.3 Improving Product Performance

ProTeqt has complete control over their mechanical locking device and deactivation tablet, but they must be compatible with many types of locking methods (e.g. USB, disk, etc.) and packaging. In the case of the USB thumb drives and the disks, the packaging is very slim, allowing the lock to be close to the deactivation tablet. Once the magnetic field is created, the lock is easily deactivated. Products that are embedded in thicker packaging (Figure 4) have proven to be more difficult to unlock because the magnetic field degrades rapidly with distance. ProTeqt has begun to investigate solutions that will permit deactivation of the mechanical lock at a distance of 1 inch from the tablet.

ProTeqt, having developed two unique applications for their technology (USB thumb drive, and CD-type disk), is ready to move forward with the development for a, new, Micro USB lock. This lock will perform similarly to the USB thumb drive lock, in that it will interface with the consumer product internally. The Micro USB port uses a smaller profile than the standard USB port, introducing some new design challenges. However, the Micro USB lock is used far more prevalently and with more expensive products than the standard USB. Moving forward, ProTeqt would like to achieve the functionality of the Micro USB lock at 1 inch above the tablet surface.

Figure 4: External hard drive with thick packaging requires a stronger field. This packaging, being targeted by ProTeqt, leaves the lock at 1 inch above the tablet.

1.4 Induction Heating

The most important concept of ProTeqt's current design is induction heating. They utilize this phenomenon to generate heat inside the lock, thereby creating a force that disengages the lock from the product. The principals of induction heating are applied from the tablet to the enabler. To simplify things, the tablet can be thought of as an induction cook top, and the enabler as a pot. The main purpose of the deactivation tablet is to heat the enabler. More information on induction heating is discussed in Chapter 2.

1.5 Resonant Coupling

As stated above, the objective of ProTeqt is to achieve unlocking at one inch from the tablet. Among several potential solutions, ProTeqt chose to explore and implement the effects of resonant inductive coupling. Resonant inductive coupling is a means to transfer wireless energy through two coils that are tuned to resonate at the same frequency. We can effectively use resonant inductive coupling to extend the magnetic field created by the deactivation tablet. In reality we can create a new magnetic field using the energy transferred wirelessly from the original field created by the tablet. Using a field that is closer to the mechanical lock will increase the effectiveness, and decrease the decaying effects of the field at distance. Furthermore, this solution will allow ProTeqt to postpone a redesign of the deactivation tablet. Instead, a simple component can be designed that will allow the wireless transfer of energy: an LC circuit.

1.6 Design and Production of LC Circuits

To increase wireless energy transfer efficiency, we need to develop an LC circuit, comprised of an inductor and a capacitor. This circuit is typically drawn as shown in Figure 5. By placing the small circuit inside the mechanical lock, we can create a new magnetic field inside the lock. The LC circuit has to be tuned to operate most efficiently at a target frequency. However, because the LC circuit will be operating inside the mechanical lock, we must consider the interaction and effects of the existing components of the lock.

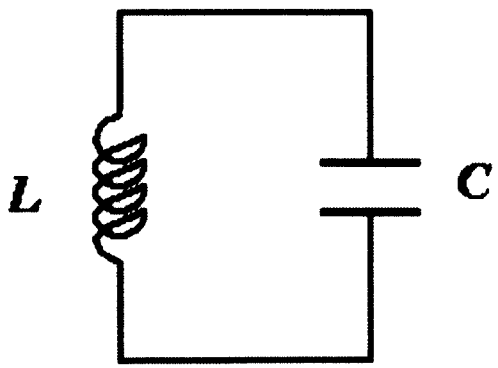

Figure 5 A typical diagram for an LC circuit where L is the inductor and C is the capacitor.

Moreover, the performance of the circuit is dependent on the quality of manufacturing. Thus, the effects of manufacturing variability must be understood, controlled, and minimized.

Finally, because the circuit is inside the lock, it is disposable and must be manufactured at low cost. The volume of the circuits is on the order of millions of units per year. The production rate and cost are two important parameters that must be considered and accounted for in the beginning stages of the design.

1.7 Problem Statement

The problem statement developed by ProTeqt for our thesis project was to understand the interactions between the deactivation tablet, LC circuit, and mechanical lock to optimize and, moreover, recommend a final design of the LC circuit that will be able to excite the enabler at 1 inch above the tablet, thereby disengaging the lock, at a manufacturing cost of $0.05.

Building on this problem statement, the goal of the project is to develop an LC circuit that will effectively extend the application of ProTeqt's benefit denial solution from zero to one inch using resonant inductive coupling. Furthermore, the forces and interactions between the LC circuit, enabler, and mechanical lock were understood to provide a better understanding of ProTeqt's entire benefit denial solution. Finally, the failure rate of the system due all the factors including manufacturing variability need to be understood and

assessed. Multiple challenges were addressed, from theoretical physics to manufacturing issues. This thesis considers the topics we faced while working at ProTeqt. It must be noted that some tasks were distributed among ProTeqt's partners and are out of the scope of this thesis.

This project was conducted through three phases. In the first phase we worked to understand, characterize, and recommend and optimal design for an LC circuit to permit the transfer of wireless energy. For this phase it was necessary to understand the principle of induction heating, the physical mechanisms required to create a new magnetic field, and the parameters for optimizing the design of an LC circuit.

In the second phase, the unlocking mechanism was analyzed to understand the interaction between the mechanical parts and the circuit. The purpose of this stage is to obtain and understand data related to the forces required to disengage the locking mechanism.

Finally, in the last phase of the project, the effect of manufacturing variability and the variability of the components in the lock were analyzed to understand the possibility of failure and the likely source of these failures.

1.8 **Task Division**

Based upon the three phases of the approach, tasks were divided among the three group members: Mitch Krogman, Amaury Rony, and myself. Even though the thesis project at hand has been completed by the collective group, each team member took the lead on one of the three phases, and delegated the responsibility for tasks essential for completion as needed. Theoretical physics and coil design was under the responsibility of Amaury Rony. Mitch Krogman led the work on the unlocking mechanism and its interaction with the LC circuit including the forces acting on and required by the lock. Finally, I took responsibility to analysis the impact of manufacturing variation on the resulting force generated by the enabler, and the possibility of failure.

2 Electromagnetism and Inductive Coupling

One key innovation of Proteqt's anti-theft system is that the locking mechanism is deactivated wirelessly via radio frequency. Electromagnetic phenomena such as induction heating and resonant coupling are implemented in the system. Understanding the physics behind the phenomena is critical for design improvement and quality control.

2.1 Principals of Induction Heating

Induction heating is a method to heat an electrically conducting object using electromagnetic induction. An inductive heater is made of an inductor excited with alternating current (AC). According to Faraday's Law, such changing current creates a changing electromagnetic field around the inductor. When the electrically conducting object is placed inside this electromagnetic field, eddy currents are generated within the conductor, and lead to Joule heating owing to losses in the conductor. Compared to traditional heating method, induction heating does not require direct physical contact as the energy is transferred through electromagnetic waves.

2.1.1 Eddy Currents

When a conductor is placed in a changing magnetic field, circulating eddies of current will be created inside the conductor. The name eddy current comes from the analogy of circulating water in fluid dynamics. In a non-zero resistivity conductor, the eddy current induced will generate Joule heating and electromagnetic forces. The current will become greater with either a stronger magnetic field or a higher frequency magnetic field. According Lenz's law, the eddy current will flow in a direction such that the magnetic field created by the current will oppose the magnetic field that induces the current. In another word, the eddy current will create a magnetic field to cancel part of the external field. During the design of the field extender, we need to be aware that adding an enabler to the field extender will reduce the current and voltage of the field extender.

2.1.2 Skin Effect

At direct current, current density is uniform through the entire cross section of the conductor. As the frequency of the alternating current increases, the magnetic field at the center of the conductor increases accordingly (Figure 6). The magnetic field creates current in the opposite direct of the current flowing through, making it more difficult for the current to flow in the center. Such resistance is called reactance. Because of the reactance at the center, the current density is the lowest there and largest near the surface of the conductor where the reactance goes to zero. This concentration of current at the surface is named the "Skin Effect".

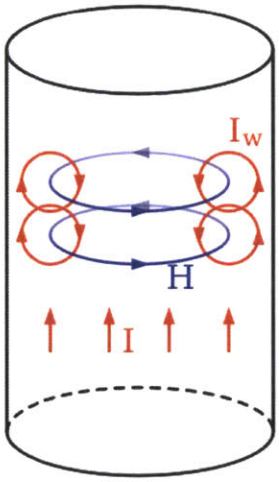

Figure 6 Schematics drawing of current and magnetic field in a conductor with alternating current. "I" is primary current. "H" is magnetic field induced. "I_w" is self-induction current.

The AC current density decreases exponentially with the depth from the surface. The skin depth is defined as the distance into a conductor at which is current density falls to 37% of its value along the surface. The skin depth can be expressed as [3]:

$$\delta = \frac{1}{\sqrt{\pi f \mu \sigma}} \qquad (2.1)$$

where:

f = frequency, μ = absolute magnetic permeability of the conductor = $\mu_o * \mu_r$,

μ_o = Permeability of air = $4\pi * 10^{-7}$ $\left(\frac{h}{m}\right)$, μ_r = Permeability of the conductor

σ = Conductivity of the material

For a copper wire with AC of 220 kHz, its skin depth will be 0.141mm. 63% of the current through a copper wire will flow within a distance of 0.141mm to the surface. The effective resistance can be calculated as current flowing uniformly through a layer of thickness δ with the DC resistivity of that material. The cross-sectional area can be approximately represented by:

$$A_{active} = \delta * 2\pi r \tag{2.2}$$

where:

r = radius of the wire

Then, the AC resistance is:

$$R_{ac} \approx R_{dc} \frac{r}{2\delta} \tag{2.3}$$

All the equations shown above are based the assumption that the skin depth is significantly smaller than the radius. However, the wire used to make the LC circuit is has diameter about 0.5 mm. The skin depth of such wire is at the same order as the wire diameter when the frequency of AC is set to 220 kHz. The AC resistance at low frequency can be calculated using:

$$R_{low\ freq} \approx R_{dc} + \frac{l}{48\sigma\pi\delta^2} \tag{2.4}$$

where:

l = total length of the wire.

Assuming same conductivity, the thinner the skin depth is, the larger the resistance is, and the stronger the dissipation or heating effectiveness will be. For this reason, in the inductor design, "skin effect" needs to be minimized by using non-ferromagnetic material such as copper. However, in the application of enabler, ferromagnetic material is better for higher heating efficiency.

2.1.3 Selection of Materials

The selection of material is critical for the effectiveness of heating. Only conductive materials can be used for induction heating because eddy current needs to flow in the object to generate heat. Even though Eddy currents can occur in any conductor, iron and its alloys respond better than aluminum and copper to induction heating owing to their ferromagnetic nature. With same alternating current, ferromagnetic materials have significantly smaller skin depth, resulting greater resistance. Therefore, more Joule heat is created.

For materials that are thinner than their skin depth at the desired frequency, the skin effect is no longer important. The resistance of the material is only determined by the thickness and basic material resistivity. In this case, aluminum and copper can perform just as well as iron.

2.2 Magnetic Field Generated by Current

This section provides an initial background on electromagnetic theory. Based on this introduction, inductive coupling is introduced. ProTeqt uses a large electromagnet in the deactivation tablet to unlock their locks. To extend their deactivation distance from the surface of the tablet to an inch above, resonant inductive coupling has been introduced to the system to permit efficient wireless energy transfer. For more extensive information, the reader can refer to a more detailed handbook [4].

2.2.1 Magnetic Field Strength at a Coil Axis

Every current, i.e. a flow of moving charges, is associated with a magnetic field with magnitude that is represented by the magnetic field strength, $\vec{B}$ (in Teslas). The magnetic field generated by a line of current within a wire is derived from Biot-Savart law [5]. That is

$$\overrightarrow{B_Q} = \frac{\mu}{4\pi}\int_0^L \frac{\vec{I}dl \times \overrightarrow{\iota_{QP}}}{QP^2} \tag{2.5}$$

where:

Q is the point of observation.

P is the center of the elementary element dl.

$\vec{I}$ indicated the intensity and the direction of the current at P.

$\overrightarrow{\iota_{QP}}$ is an elementary vector from Q to P.

$\mu = \mu_r\mu_0$ is the permeability of the medium

From this equation, it is possible to find the magnetic field along a single circular loop of radius a, carrying a current I. We are especially interested in the magnetic field $\overrightarrow{B_z}$ along the axis of the loop. It is oriented in the axis direction, as shown on Figure 7:

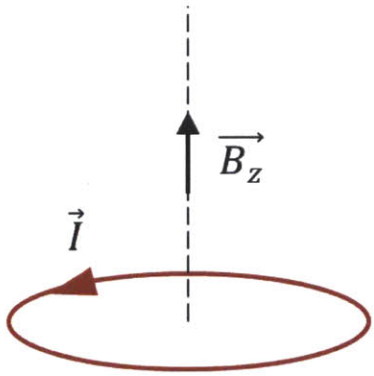

Figure 7 A current-carrying loop and it's associated magnetic field along the central axis.

The magnitude of the field is:

$$B_z = |\overrightarrow{B_z}| = \frac{\mu I a^2}{2(z^2 + a^2)^{\frac{3}{2}}} \tag{2.6}$$

To understand the effect of distance, the magnetic density is plotted as a function of the distance from the hoop (see Figure 8), which is a plot of Eq. 2.6 with a=1 m and I=1.

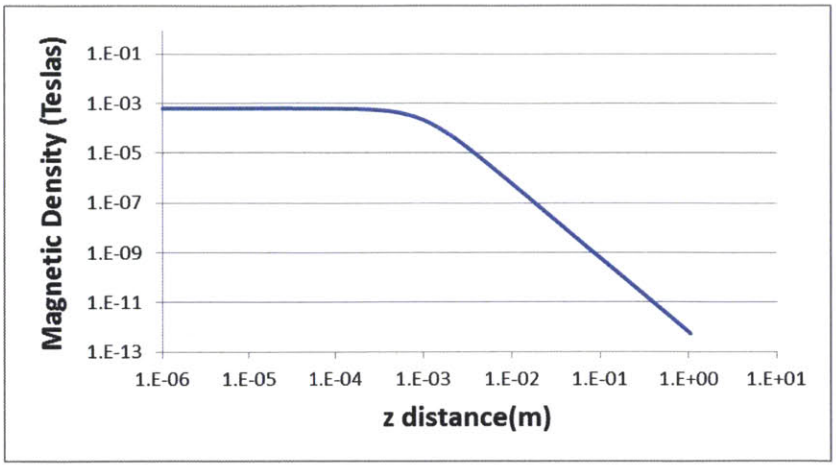

Figure 8: Magnetic Field along the hoop axis vs. the hoop radius (log-log scale). Hoop radius a = 1 mm and current I = 1A in Eq. 2.6.

As long as the distance from the conductor is less than the radius, the magnetic field remains approximately constant. However the magnetic density decreases rapidly as the measuring point is moved further away from the center of the hoop.

As will be discussed below, a flat spiral coil can be used to increase the magnetic field by increasing the number of loops. A spiral coil can be seen as a certain number of concentric hoops with different radii ($a_1, a_2, a_3 \ldots$), and potentially with N layers. In this case, the total intensity of the magnetic field along the axis of the coil is the superposition of the magnetic field intensities generated by each single loop [4].

2.2.2 Magnetic Flux and Inductance

The line along which the magnetic strength is constant is called a *line of magnetic flux*. We are interested in the *total magnetic flux*, i.e. the total number of flux lines passing through a given surface. The magnetic flux Φ is proportional to the field density B and the area:

$$\Phi = \mathrm{B.A} \tag{2.7}$$

Going back to the current-carrying hoop, it is now possible to define and calculate its inductance L.

$$L = \frac{\Phi}{I} \tag{2.8}$$

where Φ is the magnetic flux through the inside surface of the loop.

Combining Eq. (2.6) (2.7) and (2.8), the inductance of the loop can be expressed as:

$$L = \frac{\mu \pi a}{2} \tag{2.9}$$

It is noticed that inductance does not depend on the current. It only depends on the material properties and the geometry layout. The inductance of a spiral coil is the sum of the inductances of each single hoop.

2.3 Inductive Coupling

If a second conductor hoop is located closed to the first one, a portion of the magnetic flux Φ_{21} from the first hoop passes through the second. The two conductors are now inductively coupled. As for inductance (also known as self-inductance), we define the mutual inductance M_{21} of conductor hoop 2 in relation with conductor hoop 1 as:

$$M_{21} = \frac{\Phi_{21}}{I_1} \tag{2.10}$$

In a similar way, the mutual inductance of conductor hoop 1 in relation with conductor hoop 2 is:

$$M_{12} = \frac{\Phi_{12}}{I_2} \tag{2.11}$$

It has been shown that both mutual inductances are equal [4] i.e.

$$M_{12} = M_{21} = M \tag{2.12}$$

Continuing with these two coils, we consider the case where the first inductor carries a high frequency coil, producing a varying magnetic field at the same frequency. With the secondary coil located in the surrounding area so that the two are coupled, Faraday's law

states that any change to the magnetic flux generates an electric field, which induces a voltage in the secondary coil. It's this induced voltage that can be used to supply power to another application (RFID chip, transformer, etc.).

2.4 Resonant Coupling

Experience and analysis [6] show that coupling decreases very quickly as the distance between two coils increases. However, if the receiving coil is paired with a capacitor, a resonance phenomenon will increase the coupling efficiency at its natural frequency. At this frequency, the power transmission is much more efficient. Thus, the distance between the coils can be substantially increased.

2.5 Applications

The physical phenomena discussed in this chapter can be advantageously used for contactless electronic application. Two of the most important and applicable applications are RFID tags and wireless power.

2.5.1 RFID

Today many companies, large and small, use automatic identification systems, or Auto-ID, for a large range of applications; including inventory management, sales and purchase, payment, safety controls, communication, and other means. The most widely used technologies in this field are the barcode and the smartcard scanning. Among all other available solutions, RFID systems (Radio Frequency Identification) have three major advantages: identification is passive, contactless, and reconfigurable. Like smart cards, data is stored on an electronic data-carrying device, called the chip. However, RFID devices do not require physical contact between the chip and the reader. Instead, data is exchanged with an electromagnetic field. Electromagnetic waves are emitted and received through two coils, or antennas. One is connected to the chip and the other one in the reader. The chip, when accompanied by the coil, is called the transponder.

To maximize the power transmission, and the working distance between the transponder and the reader, the resonant frequency of the system is used to convey information. Two types of transponders exist today: passive and active transponders. A passive transponder does not provide energy and, instead, receives it from the reader's magnetic field. This energy causes an impedance change of the transponder: shifting the initial natural frequency of the system, which is detected by the reader. Active transponders carry a battery that allows them to transmit their ID signal using their own energy source. The signal is sent either periodically or in the presence of an RFID reader. Passive transponders are more widely used because they are less expensive, whereas active transponders are used in long distance applications [4].

2.5.2 Wireless Power Transfer

Wireless energy transfer is as old as alternating current [7]. The transformers that are ubiquitous in most electronic devices and indeed in all electricity distribution network transfer energy by using mutual inductance. In recent years wireless energy transfer for an array of application is quickly becoming an important use of resonant inductive coupling. A team of MIT physicists, and many others have been working on this subject [8,9]. They realized that resonant objects tend to couple, as opposed to off-resonant interaction, where their interaction remains extremely weak. Thus, energy transfer efficiency between two resonators increases based on the coupling level between them. This phenomenon is called non-radiative wireless energy transfer. Non-radiative energy transfer is much more interesting than other solutions, such as radiative transfer or directed radiation modes because, respectively, they produce a huge energy loss or require line of sight between transmitter and receiver. Some foreseen applications for non-radiative wireless energy are:

- Charging portable electronic devices by placing it within the source field
- Supplying power to mobile robots and machines in a factory
- Supplying power to internal medical device (pacemaker, medicine delivering devices, etc.)

Several designs have been tested and refined. Currently, the highest efficiency is achieved with a four-coil apparatus: the power supply with an inductor, first resonator, second resonator, and the receiver with the device to power (light bulb). A schematic of the system is given in Figure 9.

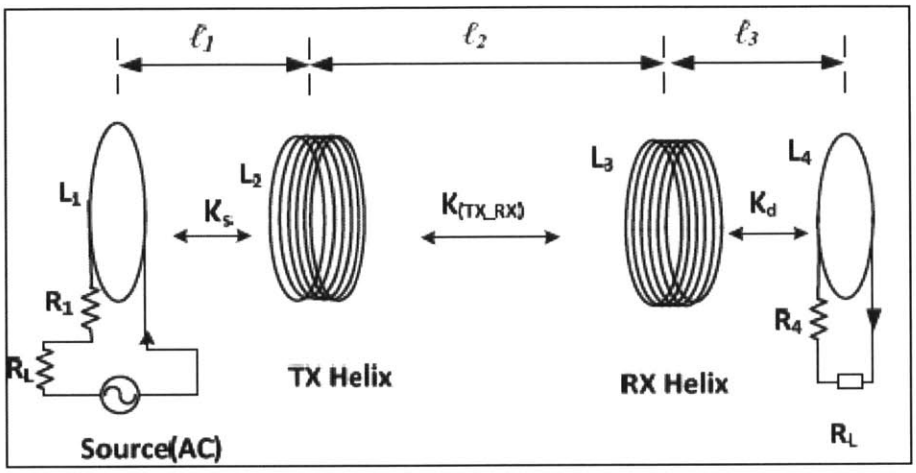

Figure 9: Typical strongly coupled magnetic resonance (SCMR) system. TX is the transmitting helix. RX is the receiving helix. [6]

In this configuration resonant inductive coupling only takes place between the two resonators. The transmitting helix is inductively coupled with the source loop. Similarly, the receiving helix is inductively coupled with the load loop. With this system, several promising achievements have been made including more than 90% efficiency at 15 cm distance, 40% efficiency with a single receiver at 2 m, and 60% efficiency with multiple receivers at 2 m. Recently, the research team, now an MIT spin-off company called *Witricity*, introduced a repeater to further increase the effective distance of the magnetic field, and thus increase the transfer distance even further by inserting another set of resonators between the two previous ones (transmitting and receiving helices). [9–11] The success of Witricity gives us theoretical foundation to develop future applications that require deactivation distance more than one inch.

3 LC Circuit Manufacturing

ProTeqt had previously determined that an LC circuit with a resonant frequency in the range of 220kHz would be necessary for wireless deactivation. This circuit would be part of each device, and therefore must be compact enough to fit in the locking device and inexpensive enough to keep the device cost low. These requirements make the design and manufacture of this circuit critical to the success of this product. In this chapter, a variety of manufacturing methods are examined for making such a device.

ProTeqt had done preliminary research to explore the design space, and found that the performance achieved by the LC circuit could prove feasible for extending the working distance of their locks to one inch. The LC Circuit can be thought of as a passive receiver. That is, the LC circuit does not contain a battery or any other power source, nor does it require its own power source to receive a signal. LC circuits can be manufactured at a very low cost because they do not contain a power source.

An LC circuit only contains an inductor (L) and a capacitor (C). Thus, manufacturing is rudimentary. One must simply join an inductor and capacitor to complete the circuit. Based on the inductance and capacitance of the two components, the natural frequency of the circuit can be predicted with the following equation:

$$f = \frac{1}{2\pi\sqrt{LC}} \tag{3.1}$$

This leaves two variables that can be changed with respect to each other, in order to achieve a certain natural frequency. The most efficient transfer of wireless energy occurs when the transmitter, or deactivation tablet, emits an electromagnetic field at the natural frequency of the LC circuit. It's here that ProTeqt would like to be in the design space.

3.1 Inductor Manufacturing

An inductor, in its simplest form, is a coil of wire used to resist a non-constant current flow [12]. It stores energy in a magnetic field created by current flowing through a coil. Inductors come in many shapes and sizes. These parameters often affect inductor performance [13]. The magnetic field created by an inductor is dependent on inductor shape, whereas the intensity of the field is determined by the number of turns within the coil. For our application we are interested in designs that will permit an electromagnetic field extension through resonant coupling. Materials are especially important in inductors. The time required to establish a magnetic field is proportional to the coil resistance. High current is desirable to quickly set up a magnetic field. Changing the linear length of the coil, or the coil's material properties can alter resistance, and therefore the field [13]. High coil resistance will also result in heating, and therefore promotes energy loss. For this project, three possible inductor-manufacturing methods were: coil winding, chemical etching and screen printing.

3.1.1 Chemical Etching

Chemical etching is a controlled material removal process that uses a resist to prevent portions of a material from being removed by a chemical etchant. Once the resist is removed, a desired pattern remains (Figure 10). The process at hand uses copper and a resist to etch a copper pattern.

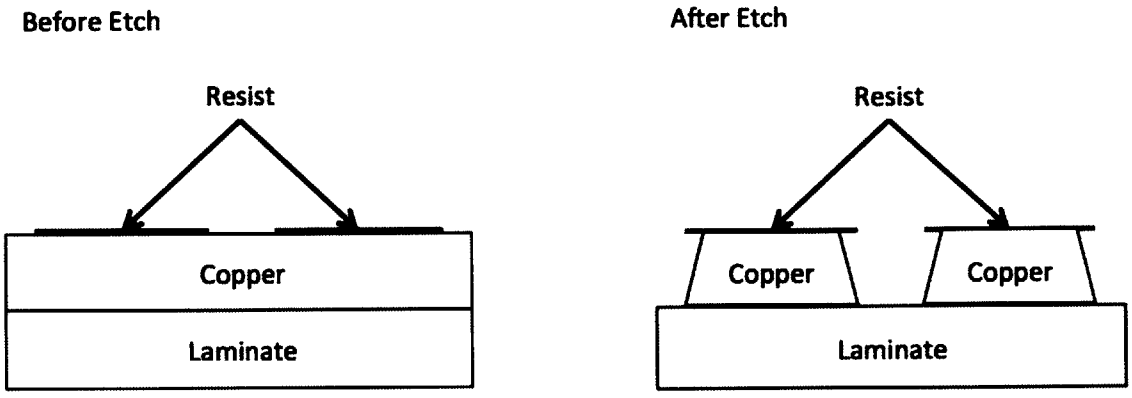

Figure 10 Schematic of a typical etching process.

Figure 10 explains how chemical etching works [14]. You will notice that the etchant removes material in both horizontal and vertical directions. That is, a slight angle is apparent in the final product because the etchant is in contact with that portion of the material after it passes beyond the resist. Finally, it's important to note that this is a chemical material removal process. Meaning the copper that is removed cannot be easily recycled, making the process as a whole, inefficient.

Etching allows for batch processing of inductors. However, it restricts coil designs to single layer, flat spiral coils. Economical etching is usually done in large batches of very thin materials. These materials are often on the order of 0.03mm thick [14]. As material thickness increases, time to etch and removed material both increase. This property is inefficient in terms of processing energy and material usage. It directly impacts the production cost.

As material thickness decreases, resistance increases. This resistance restricts current flow through the material, and therefore increases the amount of voltage needed to create an electromagnetic field. The time requirement to etch thick pieces of copper (0.5mm) is about 5 minutes [15]. This however is not what limits the chemical etching process in terms of this application. The limiting factor is in the material costs. Copper is very expensive, and is only one of the materials used in the process. Resist and the chemical etchant also need to be purchased, along with the many cleaning solutions used to remove the etchant.

3.1.2 Coil Winding

Coil winding is a process that bends a wire (usually radially) into a desired shape. This can be done manually or automatically, and many different winding patterns can be achieved. This process bodes well for inductor manufacturing because an inductor, in its most basic form, is a wound coil. Size and shape of the coil, and wire used to create the coil can impact the inductor performance. Wound coils can be formed into almost any desired shape including flat spiral, cylindrical, rectangular, etc. Wire geometry is often limited by market availability. Rectangular and circular cross sectional wire are most common. Wires are found most commonly in certain AWG gage sizes, which have a

circular cross section. Diameters are fully customizable depending on the type of winding machine. Usually machines can operate using a range of wires. Automatic machines often integrate several functions including dispensing, winding, and cutting the wire. Machines can accommodate simultaneous coil winding, providing a batch process. Batch processing allows the machines to produce coils at a high rate. The cost of copper wire is relatively low compared to silver ink [16]. Wire is packaged as a large spool that is fed into the coil-winding machine. Because the wire is continuous, there is almost no waste of copper compared to chemical etching. The two ends of each coil are left exposed, ready to be soldered to the remaining capacitor.

3.1.3 Screen Printing

Screen printing is a highly integrated manufacturing process that can provide an entire LC circuit in one process. The process uses a mask that contains the circuit pattern. Conductive ink is then deposited on the mask, and the circuit is printed on the areas not protected. Silver and Aluminum are the most popular conductive inks used in this process. Dielectric materials can also be used to print capacitors. This is done in layers. First a silver layer is deposited, followed by a dielectric, and finally another silver layer. [17]

The flexibility of screen printing is similar to that of chemical etching. It is commonly used for making flat, flexible circuits. The deposited layers are very thin (40 micron), but can be built up in layers. Building layers requires more processing time, and is therefore less economical. The thin nature of screen printing causes inherently high resistance values. Capacitors are printed as large flat surfaces, requiring a large amount of surface area. Spacing is also critical in screen printing. The silver ink does not have an insulating coating, so line spacing also requires more space. Like chemical etching, large batches can be printed at once. However, screen printing requires no post processing because the capacitor can be printed as part of the circuit. [17]

The screen printing process is relatively new when compared to processes like etching or winding. While the added flexibility and integrated components are great for circuit board design and manufacture, it is still a new processes, and therefore costly. Even at the

materials level, silver ink is much more expensive than copper for a given volume. While this process isn't right at this time, future developments could lead to significant cost reduction, leaving it as a potential process for future manufacturing. [17]

3.2 Capacitors

Capacitors are common electrical components used in many types of circuits. They consist of two conductive plates that are separated by a dielectric layer. This configuration allows capacitors to hold a charge. Capacitors come in many shapes and sizes due to their simple design (**Figure 11**). Capacitors are made in extremely high volumes by expert manufactures. With their cost at $0.0074/capacitor[2], ProTeqt will be purchasing capacitors to use within their circuit.

Figure 11: Typical shapes and sizes of capacitors.

Capacitor specifications usually include three key pieces of information: nominal capacitance and rated voltage. A capacitor will likely have these values printed on its side. A capacitor reading 1μf, 20% at 100V, for example, will have a nominal capacitance of 1 microfarad with a tolerance of ± 20% (0.8μf – 1.2μf). Throughout the life of the capacitor, it should not handle more than 100 volts, as that is the rated voltage.

[2] Fenghua Electronics, Part number 0805M for quantities of 10,000 pieces

3.3 Soldering Techniques

Soldering is a method of joining two thin metals using a filler material. This filler material has a lower melting temperature than the two thin metal pieces, allowing the filler material to flow between, and bond to each of the thin metal pieces. The filler material is often made of tin and lead. Conductive properties allow soldering techniques to be prevalent in the electronics manufacturing industry, and especially circuit board manufacturing. Two common soldering methods are used in manufacturing today: robotic soldering and dip soldering.

Robotic soldering often uses a robot or other automation to control temperature and the feed rate of the filler material. Sophisticated control systems are used to gain a high level of precision over soldering processes. Robotic soldering often requires auxiliary tooling or methods of positioning and orienting components before they can be soldered.

Dip soldering is used more extensively for circuit board manufacturing. This process is used to solder several components simultaneously. Leads from electrical components protrude through the bottom of the printed circuit board. These are dipped into a lead-tin bath, where the solder then solidifies upon removal. [18]

3.4 Preliminary Comparison of Processes

Coil winding was the manufacturing process chosen to perform design optimization and manufacturing variability analysis in this project. Three manufacturing methods: winding, etching and screen printing were chosen to conduct a preliminary comparison. The comparison is based on three criteria: design feasibility, cost, and manufacturing feasibility.

Based on the testing done by the engineers at ProTeqt, a hand made winding coil had proved to be working. The coil was made of AWG 24 copper wire, with 9 turns. It had an oval shape to maximize its surface area. The detailed dimension of the coil is shown in Figure 12.

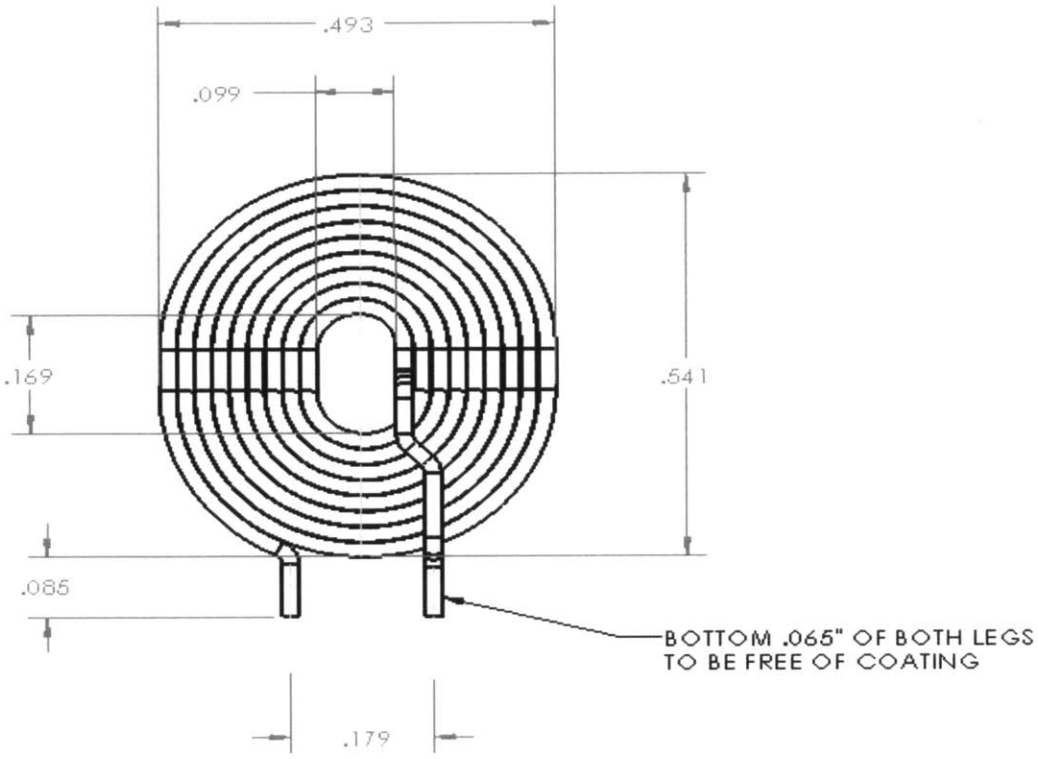

Figure 12 Drawing of a Machine Wound Coil

The Q factor is the inverse of the damping ratio of the resonant circuit, and thus a measure of the amplification of the input that occurs at the resonant frequency. It is a key metric to evaluate the energy transfer efficiency of an LC circuit, and can be expressed in equation:

$$Q = \frac{R}{2\pi f L} \tag{3.2}$$

where:

R = resistor, f = natural frequency, and L = inductance.

The Q factor of this circuit at 200kHz is about 35. Among the three potential manufacturing methods, winding is the only process that can produce a coil with comparable Q factor while being highly manufacturable and low cost. For etching and

screen printing, however, the resistance of the coil is significantly higher due to the small thickness. Metal foil used in etching is normally on the order of 0.03mm thick [14]. Thicker foil will increase cost and the manufacturing time. Thickness of screen printing pattern is normally below 100μm [19]. Multiple-layer is feasible, but just as increasing the thickness of foil in etching, it will raise both cost and process time. If we reduce the number of turns to achieve low resistance, inductance will decrease as it is positively related to the number of turns.

In addition to the design challenge, the manufacturing cost of etching and screen printing is significantly higher than winding. Etching being a fairly complicated process requires higher equipment investment and complex procedure. Material waste of etching is much higher than coil winding as it is a material removal process, while coil winding being a continuous process has very little material waste. Silver price was about $800/kg comparing to $7/kg for copper during this project[3]. Therefore, for screen printing, even the cost of ink alone is much higher that the 5-cent cost constraint.

Taking all the factors into consideration, coil winding was the manufacturing process chosen to perform design optimization and manufacturability analysis in this project.

3.5 Wound Coil Cost Analysis

Cost is the major constraint for selecting a manufacturing method. The cost estimate of manufacturing a wound coil can be broken down into three components: machine cost, labor cost and material cost. A baseline analysis of cost can help ProTeqt choose a manufacturing method and negotiate price with vendors.

According the quote from winding machine manufacturer Wey Hwang Co., the price of a fully automatic coil-winding machine is $20,000. The depreciation of the machine is amortized into five years. One machine can manufacture 500 coils per hour based on the specification. Labor cost is estimated at $5/hour using shifts that cover 16hours per day at 300 days per year. We assume that one laborer can take care of 5 machines. The material

[3] Commodity futures price (COMEX) from nasdaq.com

is comprised of wire, solder and capacitors. The price of copper wire is highly dependent on the market price of copper. The wire price is set to $10/kg [16]. Based on the assumptions made, each coil costs 0.46 cents in material, 0.2 cents in labor, 0.16 cents in machine and 0.82 cents total. According to the electronic component manufacture Fenghua, a 20% ceramic capacitor rated at 1μF, 100V is priced at 0.74 cent. Assuming 1 cent for the soldering process, the total manufacturing cost is 2.56 cents.

Other cost such as administration, facility and distribution were not included in this model. Given the fact that material is the major cost in this industry, we expect the total cost to be within the target of 5 cents.

4 Coil and Circuit Design

By the time this project started, ProTeqt had developed coil design that works at one-inch distance above the deactivator tablet. However, the physics behind the success was not well understood, and whether or not a better design exists remained unknown. The objective of this section is to provide design recommendation of the coil, which maximizes the energy transfer between the tablet coil and the LC circuit. Preliminary experiments were first been conducted to identify the significance and the interaction between the parameters of the system, especially between the two coils (distance, number of turns, wire gage...). Then a theoretical analysis was performed, using the information from Chapter 2. The result of this analysis was then compared to a series of experiments done at ProTeqt. In order to extend this work to other manufacturing processes, an alternative design in the case of thin wires (when cross section area is below typical copper wires) is described in Appendix A.

The final design is subject to some geometric constraints as the design of the micro-USB lock housing has already been done. Thus, the size of the LC circuit has to be within the interior space of the housing in order to fit inside the lock. The space for the circuit consists of two empty parallelepipeds: one for the coil and one for the capacitor (see Figure 13).

For more detailed design process, please refer to Amaury Rony's thesis. [20]

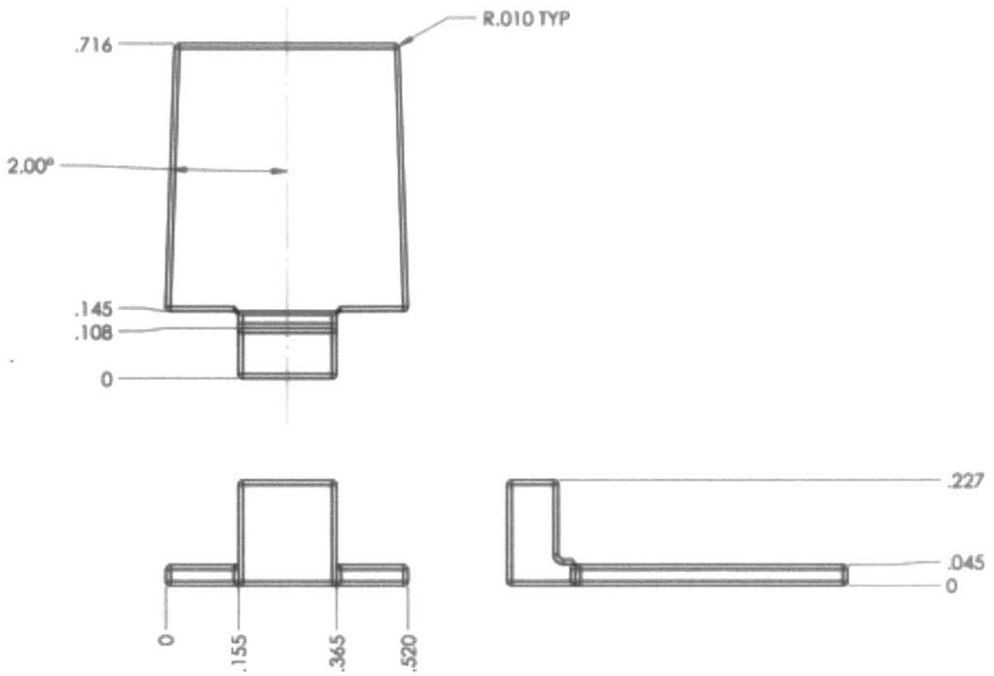

Figure 13 Usable volume (in inches) inside the lock, dedicated for the LC circuit.

4.1 LC Circuit Experimentation

The inductor and capacitor share a relationship that can be optimized in order to create the most effective field, thereby heating and expanding the enabler. The most important design component is the inductor because it must act as an antenna and generate it own field. The inductance depends on the geometry of the coil, such as the wire gage size and number of turns in the coil. Once the inductor geometry is optimized, a capacitor can be chosen to target a certain natural frequency for the circuit.

To find the optimal inductor geometry, a design of experiments was conducted to generate a response surface based on the wire gage and number of turns in the coil. The measured output of this test was voltage, which was converted to current based on the known resistance of the coils using equation:

$$I = \frac{V_{pp}}{\sqrt{8(R^2 + (2\pi f L)^2)}} \tag{4.1}$$

where:

Vpp = the peak-to-peak voltage measured, R = resistance of the coil, f = frequency, L = inductance of the coil.

To conduct the experiment, a primary coil was connected to a function generator and amplifier, and placed below a surface representing the deactivation tablet. Above this setup, six different circuits with different inductor geometries were connected to an oscilloscope in order to measure the peak-to-peak voltage. From here the values were converted into current. The current in the coil should be maximized in order to create the strongest magnetic field, and therefore generate the maximum amount of eddy currents to heat the enabler.

The deactivation tablet has been optimized to operate around 220 kHz. To keep the natural frequency at this target, we measured the inductance of each coil, and then paired it with the proper capacitor. After generating the response surface, the inductor geometry was optimized based on the geometric lock constraints. The capacitor was selected based on the inductor. The pairing of the two components led to the optimal circuit design of the LC circuit.

Using the optimal design, experiments were conducted to understand the coupling efficiency between the two coils. We defined efficiency as the ratio of output current in the LC circuit (I_{load}) over the input current to the primary coil (I_{source}):

$$Eff = \frac{I_{load}}{I_{source}} \tag{4.2}$$

To obtain the current, voltage was measured in both the primary circuit and the LC circuit, and then converted to current using Eq.(4.1). The efficiency of each coil then was calculated accordingly. Finally, same test was conducted with full-sized and half-sized enabler placed on the LC circuits. The goal is to understand the effects of placing the circuit inside the lock on the efficiency of the coupling between the primary coil and the LC circuit.

4.2 LC Circuit Optimization Results

4.2.1 Optimal Secondary Coil Design

By testing six coils with varying gage size and number of turns, we gathered data and generated a response surface that would help us to predict the performance of any other combination of gage sizes or number of turns. According to the response surface in

Figure 14, the wire gage and number of turns in the coil should be maximized to generate the most current. Larger gage size wire has lower resistance and thereby higher resulting current. Also, increasing the wire gage corresponds to a shorter wire. Two coils that have the same outer diameter but different gage sizes, the larger gage size coil would have a shorter unwound wire, which again decreases resistance and increases current flow.

With a general understanding of how current corresponds to a coil design, other constraints were considered in order to fully optimize the circuit. It was found that the largest gage size fit within the given volume of the lock was AWG 24. This wire diameter is around 0.5 mm. This is the maximum gage size because the wire must be routed in and out of the flat spiral coil, effectively requiring us to cut the allowable height in half. With the wire gage in place, the maximum number of turns was 9, when leaving an appropriate inside diameter for the manufacturing of the coils.

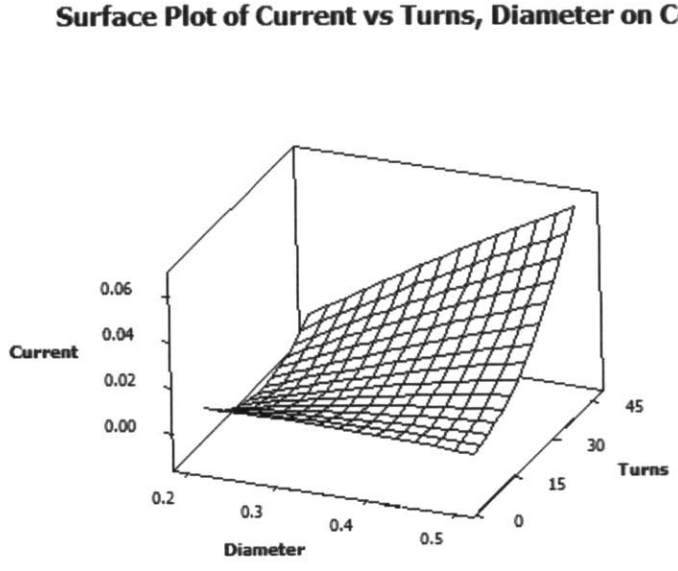

Figure 14: Response surface in current for various coil characteristics.

A theoretical model was created to confirm this design. Table 1 shows the optimal coil using the theoretical model. The output of the model is current (A). For more on the theoretical model, please see Amaury Rony's thesis. [20] From the table we again gather that optimal design for the inductor coil uses 24 AWG wire for a coil with 9 turns.

Table 1 Circuit design optimization result from a theatrical model. The grey area is the ones that exceed the space constraint. The optimal combination is highlighted with solid border (AWG 24 and 9 turns). Highlighted in dash-line borders are two possible combinations with slightly larger interior space.

AWG \ Turns	6	7	8	9	10	11	12	13
22	4.76	5.29	5.82	6.36	6.90	7.45	7.99	8.54
23	3.56	3.94	4.31	4.69	5.07	5.45	5.83	6.21
24	2.68	2.94	3.20	3.47	3.73	4.00	4.27	4.54
25	2.03	2.21	2.39	2.58	2.76	2.95	3.14	3.33
26	1.53	1.66	1.78	1.91	2.04	2.17	2.30	2.43
27	1.17	1.26	1.35	1.44	1.54	1.63	1.72	1.81
28	0.89	0.95	1.01	1.07	1.14	1.20	1.27	1.33

Moving forward, a capacitor had to be joined to the coil to complete the LC circuit. The capacitance was calculated using Eq.(3.1) using the inductance and target frequency of an LC circuit. With the tablet being optimized to operate around 220 kHz, we could back calculate a capacitance value for the inductor so that the natural frequency of the LC circuit would be 220 kHz. A 1μF capacitor was included in the final specifications for the circuit, because it's the most common capacitance value near the theoretical value calculated using the formula.

4.2.2 The Quality of Coupling and the Effect of Enabler

With the final specifications of the circuit design in place, the circuit was analyzed to understand the coupling efficiency. Using the methods discussed above, we were able to obtain plots of the ratio of current out of the secondary coil vs. the primary coil, or efficiency, and understand how that changed with the frequency. Figure 15 shows a

coupling efficiency plot of the optimal circuit (AWG24, 9 turn, 1μF) at one-inch distance.

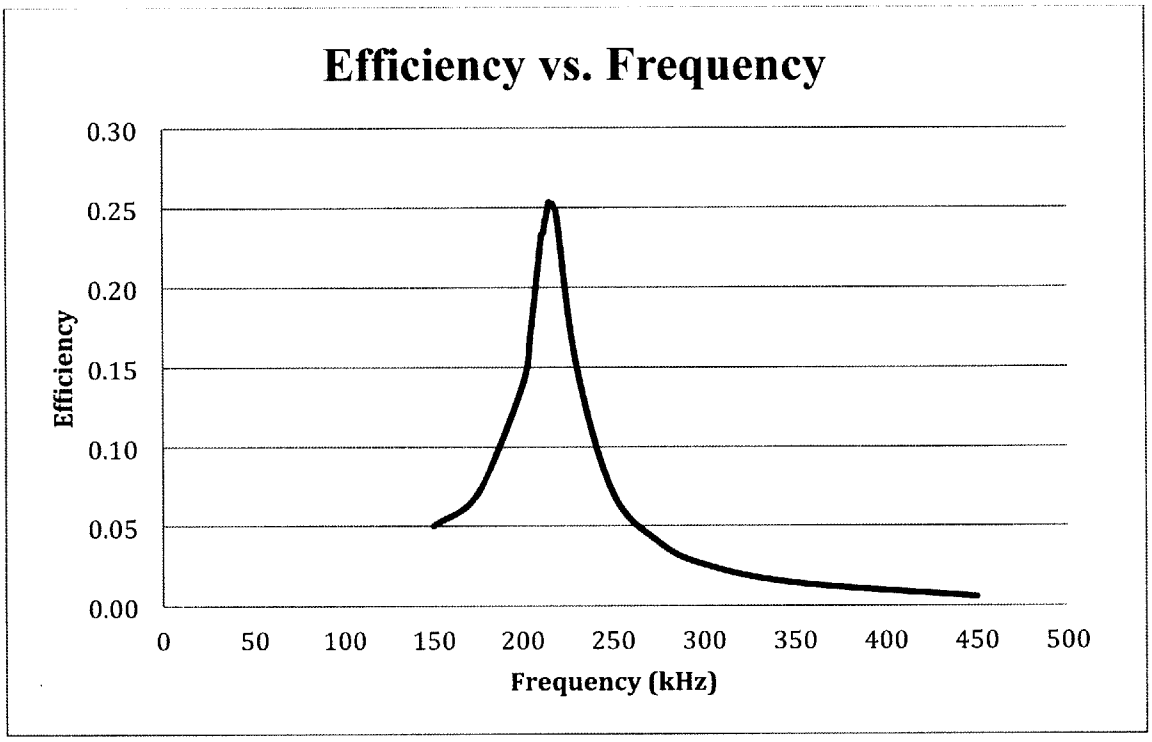

Figure 15: Efficiency vs. Frequency plot for the optimal LC circuit.

Notice the large spike in efficiency around 200 kHz. It is the natural frequency the LC circuit is tuned to. At this frequency, the circuit has the highest effective wireless energy transfer.

The next step was to test the circuit to understand the effects of the other metal components in the lock. The concern was that other conductive materials inside the lock could shift the natural frequency of the circuit if within a close proximity. It was found that the enabler had an extreme dampening effect on the coupling efficiency of the circuit. This meant that, while the enabler did expand, it did so using much less wireless energy than expected. Figure 16 is a plot comparing the efficiency of the LC circuit with and without the enabler.

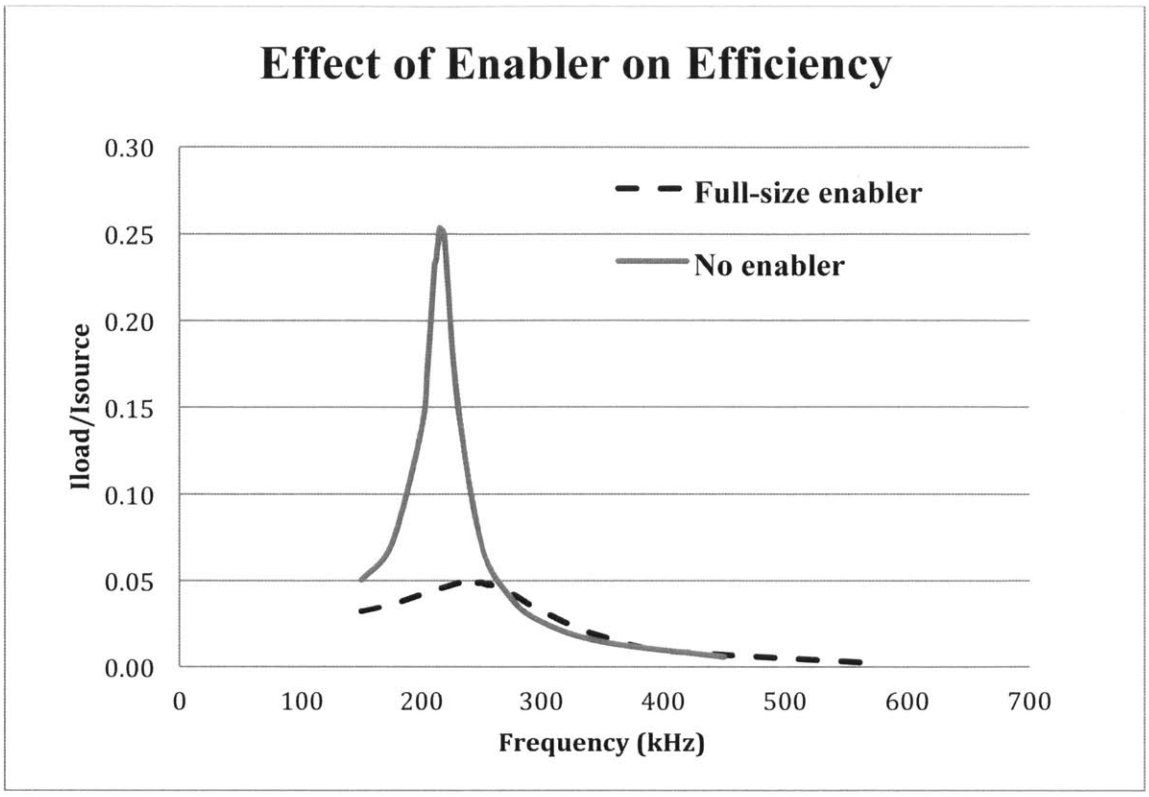

Figure 16: Efficiency vs. Frequency plot for an LC circuit with and without a full sized enabler.

Figure 16 shows that the enabler dampens the efficiency of the wireless energy transfer by about five times. The natural frequency is also shifted from 200kHz to 235kHz. To further understand the effects, a half sized enabler was analyzed using the same method. It was found that the efficiency was still dampened, however the extent was significantly less. This effect can be seen in Figure 17.

Some deactivation tests were done using the optimal circuit, and the lock was disengaged successfully most of the time. It can be concluded from the circuit design modeling and testing that the optimal coil design is feasible for the application at one inch.

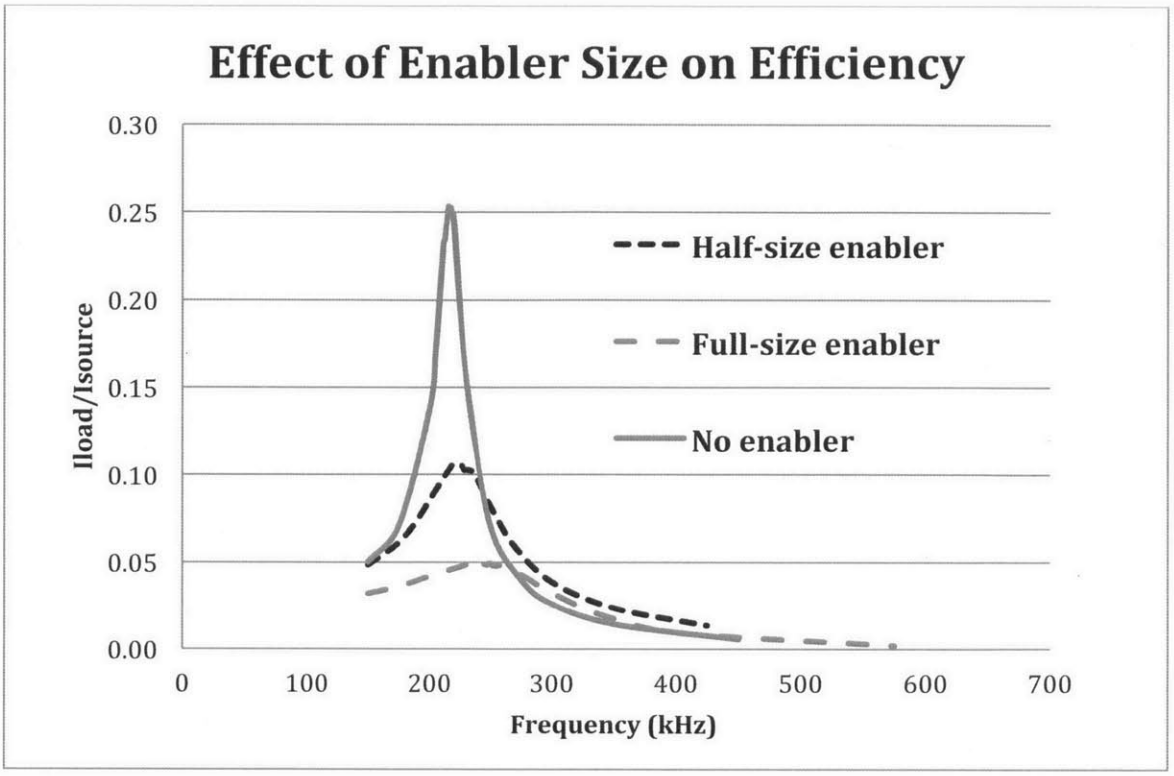

Figure 17: Efficiency vs. Frequency plot for an LC circuit with and without a full and half sized enabler.

5 Mechanical Lock Analysis

The success of the lock system requires the force generated by the enabler to be greater than the force required to disengage the mechanical lock system. The mechanical lock system analyzed throughout this thesis is a micro USB lock system, which has been identified as a critical mechanism that will facilitate growth and opportunities for ProTeqt. The objective of the analysis on the mechanical lock is separated into two parts. First the forces required to disengage the lock should be understood, followed by the forces that can be achieved by the enabler at a distance of zero and one inch. The optimal circuit (AWG 24, 9 turns, $1\mu F\ capacitor$) developed in the coil design phase was used in this force test. For more detailed about the test, please refer to Mitchell Krogman's thesis. [21]

5.1 Mechanical Lock Force Analysis

To better understand the forces required by the lock to disengage, three analyses were completed: analytical calculation, finite element analysis (FEA), and empirical data collection. The analytical model and FEA model are simplified model of the real lock based the CAD drawing. Analytical model can provide a theoretical baseline to validate the result from FEA model. However, only the measurement data can represent the actual force needed to disengage the lock. Knowing the results from all three methods could help us understand the manufacturing precision of the parts.

5.1.1 Analytical Calculations

An analytical calculation was used to understand the forces required to disengage the lock. This analysis used a typical beam-bending model (Figure 18) and a sliding friction model to calculate the forces required by the lock:

$$F_{Total} = F_{Friction} + F_{Bending} \tag{5.1}$$

$F_{Friction}$ can be defined as:

$$F_{Friction} = \mu F_{Spring} \tag{5.2}$$

where μ = the coefficient of friction between the two stainless steel components.

$F_{Bending}$ can be defined using the following model:

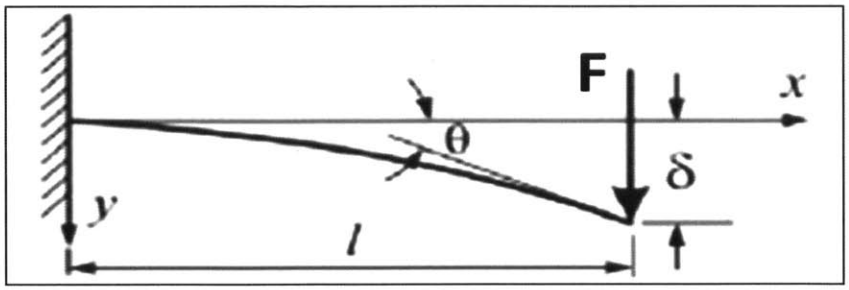

Figure 18 Beam Bending Model used for Analytical Calculations

$$F_{Bending} = \delta(x)\frac{6EI}{x^2(3L-x)} \tag{5.3}$$

where δ(x) = displacement at point x, E = Young's modulus of the sheet metal,

I = inertia, l = length of the beam, and x = position at which the force is applied.

5.1.2 Finite Element Analysis (FEA)

In order to fully understand the interactions and forces required inside the lock, an FEA was conducted to gather numerical result of the bending force required. The FEA was completed using 3D data of the most current lock design. Solidworks Cosmos was used to conduct the analysis.

The model is simplified, focusing on the force required to bend the sheet metal component shown in Figure 19.

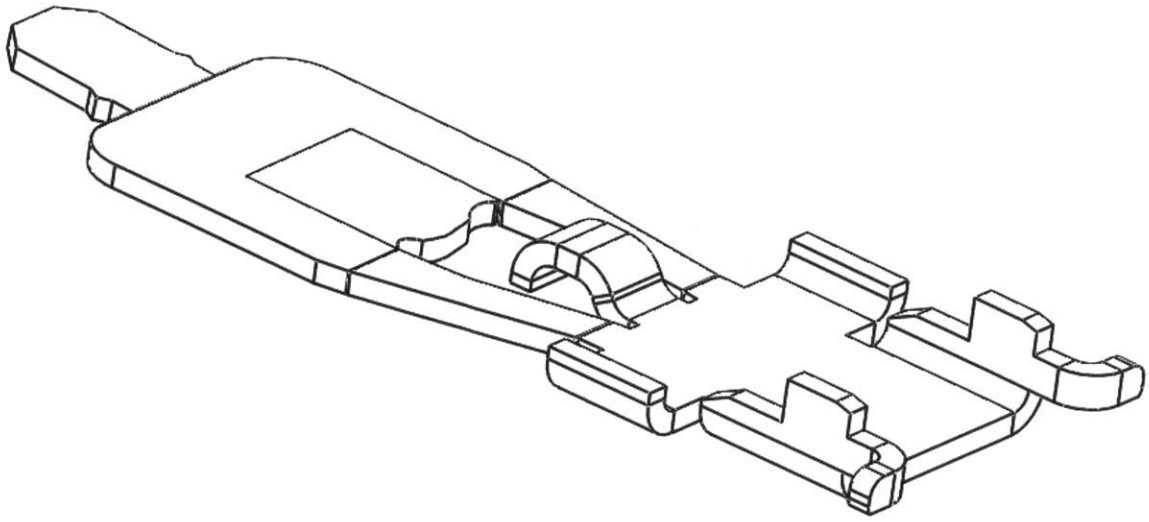

Figure 19 Image of the First Sheet Metal Component.

The majority of this component is housed inside of the other sheet metal component (sheet metal 2). Stainless steel was used for both sheet metal parts. For detailed description about the interface between the two sheet-metal parts, please refer to Chapter 1.3.2.

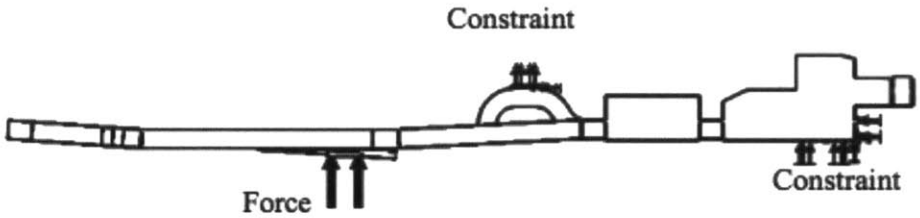

Figure 20 Constraints and Loads as Applied in the FEA

To obtain the results of the FEA, we applied varying levels of force until we reached 0.5mm of displacement. At 0.5mm the two pieces clear each other, allowing the first metal piece to be forced through the sheath by the spring. Figure 20 is the model prepared for the analysis. The small arrows signify points of fixation whereas the larger arrows on the left represent the force.

5.1.3 Empirical Test

The first two analyses used to obtain the force required to disengage the lock provide an initial[1] level of understanding. To gain a true perspective of the force required, a test procedure was implemented to capture the force required to disengage the lock.

To facilitate testing, one side of the external housing was removed, leaving the internal components exposed. The plastic component, LC circuit, and enabler were removed for testing. This allowed enough space to access the sheet metal components using a probe fastened the end of a force gage. The spring remained inside the lock throughout testing to provide results that were similar to real situation. The measurements are a sum of the forces due to friction and bending.

To facilitate repeatability, the force gage was fixed and set to zero before each test. The lock was then positioned so that the probe on the end of the force gage was directly on the sheet metal, as to mimic the plastic component. As the lock is brought closer to the force gage the force increases until, finally, the lock disengages. When the lock is disengaged the force drops back to zero. The force gage is able to record the peak force throughout the unlocking process, which is the recorded measurement for the empirical test. In total, 30 data points were measured.

5.2 Enabler Force Analysis

The force required to disengage the lock in turn determines the minimum force required from the enabler. If the force produced by the enabler does not exceed the force required by the lock, it will fail to disengage. The shear number of products that could eventually be facilitated by ProTeqt's technology leaves little to no room for error. Accordingly, experiments with full-size (9mm x 12mm) and half –size (9mm x 6mm) enablers placed on both the surface of the tablet and one inch above were conducted to gain a better understanding of the forces produced by the enabler.

5.2.1 Experimental Apparatus

The experimental apparatus was designed to reliably measure the force created by the enabler while maintaining a level of flexibility to change various parameters. The force

gage for resulting force measurement was attached to a rigid wood frame (**Figure 21**). The horizontal beam of frame could move vertically if needed to facilitate experiment at different height.

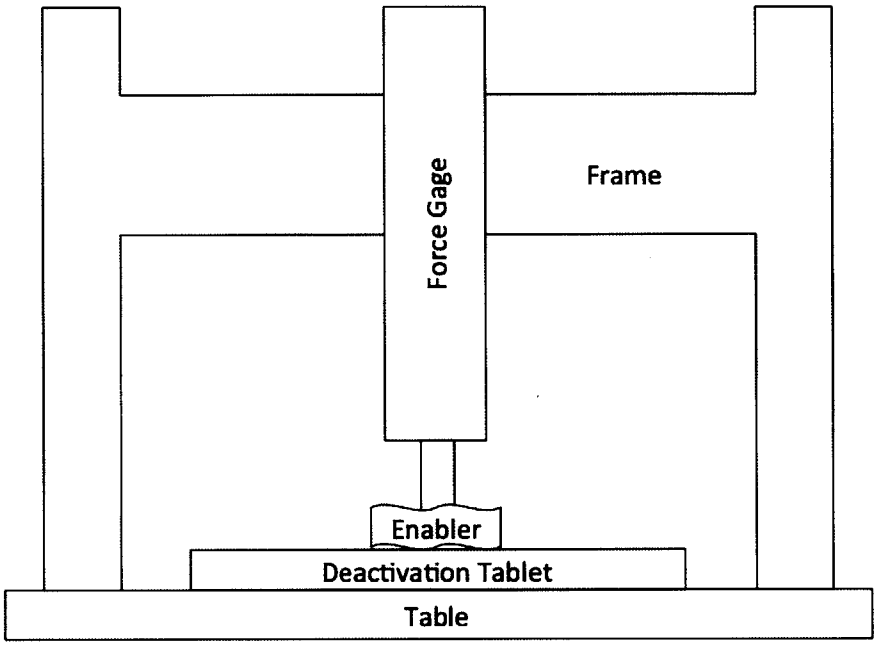

Figure 21: Diagram Explaining the Enabler Force Test Setup.

In order to accurately represent the constrained space inside the lock, a Lexan fixture was used to constrain the enabler (**Figure 22**). It was laser cut with pockets of various sizes in which enablers with different sizes were placed. Thin cardboard pieces were placed in the pocket. By changing the number of cardboard pieces, the vertical space inside the pocket could be adjusted. Another piece of Lexan was placed on top of the constraining fixture for consistent measurement and protection of the force gage.

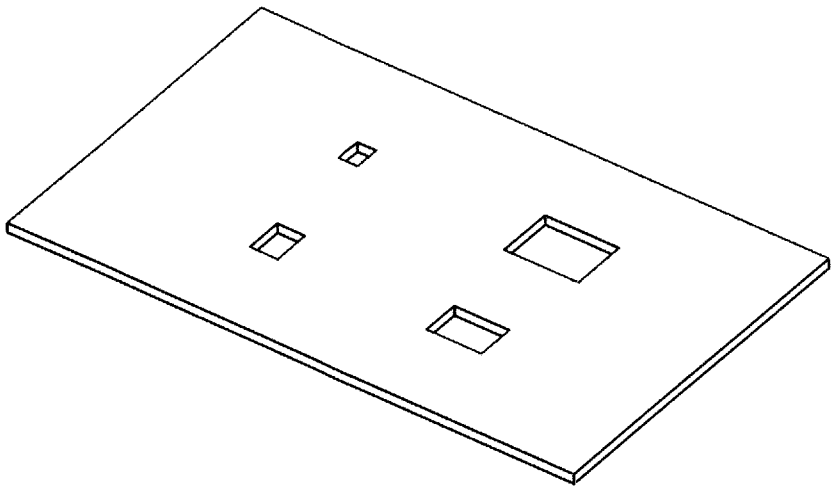

Figure 22: Model of an Enabler Constraint Fixture

5.2.2 Preliminary Analysis

A number of tests were conducted to understand the different parameters and components that ultimately lead to the resulting enabler force at zero and one inch.

Optimal Processing Time

An analysis of processing time (time duration that the deactivation tablet produced the desired field) was conducted to find the optimal processing time to process all proceeding experiments. Disengagement of the lock should use less than one second. This constraint has been set as per request from ProTeqt's potential customers. To understand the effect of deactivation time on force, five samples were taken at intervals of 0.1 seconds from 0.1 to 1 second. For full-size enabler on the tablet, the data was shown in **Figure 23**. The instrumentation could not detect a change in force from 0.5 to 1 second, so only data from 0.1 to 0.5 seconds were shown. The force generated reaches its peak with processing time of 0.3 seconds. However, this force has a high standard deviation, which continues to be a trend through 0.4 seconds. In the test, we observed that for duration longer than 0.3 seconds, some of the test enablers were burned randomly, resulting much smaller forces. 0.2 seconds was chosen as the optimal processing time on the tablet because it provided sufficient force for measurement with small variation.

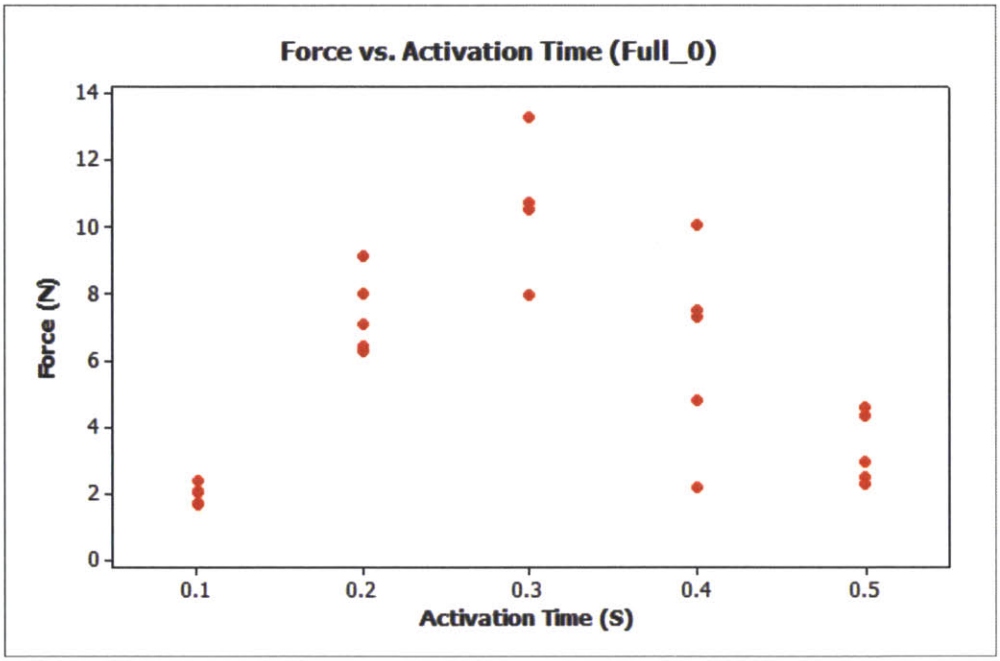

Figure 23: Individual Value Plot of Force vs. Activation Time Using a Full Enabler with Zero Distance from the Surface of the Deactivation Tablet.

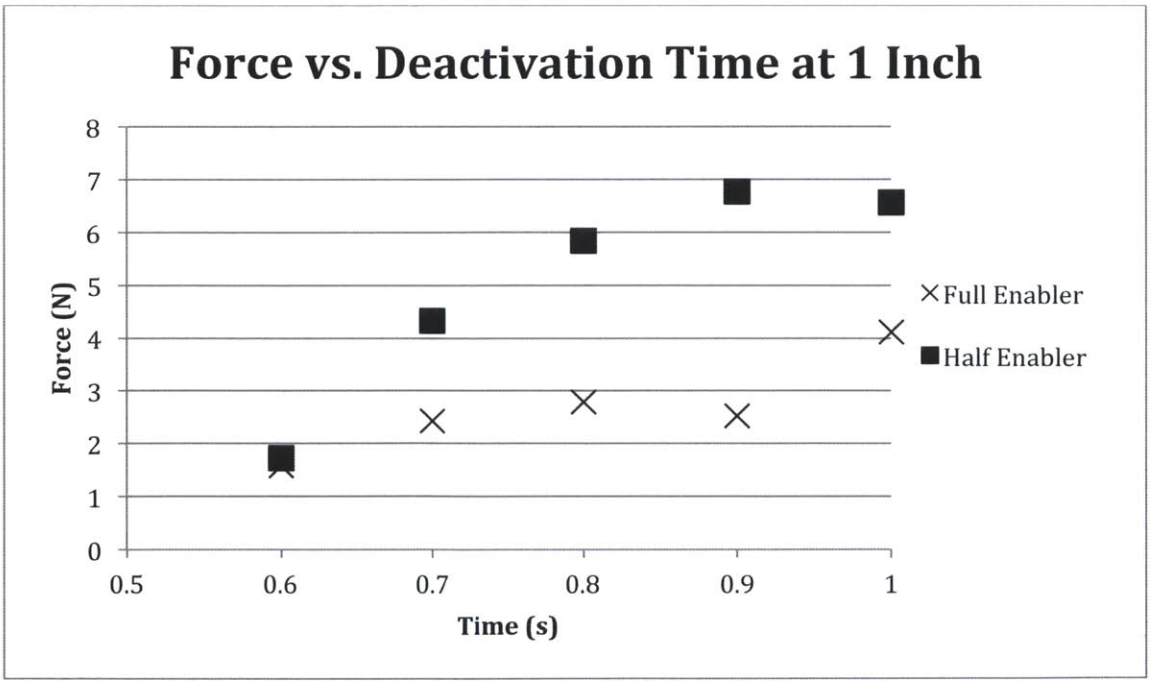

Figure 24: Force vs. Deactivation Time at 1 Inch Above the Deactivation Tablet.

At the one-inch distance, the same tests were conducted. As shown in **Figure 24**, both sizes of enablers needed much longer processing time when far away from the surface even with the help of the LC circuit. Maximum force was reached at around one second for both types of enablers, and they were just large enough for measurement. Therefore, the processing time for test at one-inch distance was set to one second. Processing time for all the tests is shown in Table 2.

Table 2 Optimal Processing Time for Enabler Force Experiment

	Enabler size	Processing Time (sec)
On tablet	Full	0.2
	Half	0.2
1 inch above	Full	1
	Half	1

Space Constraint

With a fixed time, the effects of constraining the enabler both vertically and with respect to its perimeter were analyzed to predict performance within the lock, given certain dimensional constraints and tolerances inherent in the manufacturing processes. By adding cardboard pieces, vertical constraint was controlled. Two lateral constraints were achieved by using different size pockets. One had the exact size as the enabler, and the other one has 1mm clearance on each edge. The test result of full-size enabler on the tablet is given in Table 3.

Table 3 Average force for different levels of confinement (full-size enabler, on tablet)

Vertical / Lateral	1 piece (0.43mm)	2 piece (0.86mm)
Exact	6.2N	11.1N
1mm of clearance	N/A	6.1N

Ideally the enabler should be under full confinement to generate the maximum force. However, to push the locking mechanism, the enabler has to have about 0.5mm of

vertical displacement. Therefore, in the enabler force test, only one piece of cardboard was inserted to give 0.5mm of vertical clearance, while the lateral space was fully constrained.

Size of the Enabler

Tests on the tablet and at one inch were conducted to understand the effects of using a half-size enable comparing to a full-size one, as recommended to increase the coupling efficiency between the primary coil and the LC circuit. The test on the tablet was used as a baseline to explore the difference between the forces generated by enablers of different sizes under the same condition. Thirty data points were taken for each enabler size. Then, a comparison test was done at one-inch distance with five data points for each enabler size. The LC circuit with optimal design was implemented in this test.

The test result is exhibited in Table 4. The data suggests that the full enabler produces more force than the half sized enabler when expanded directly on the surface of the deactivation tablet. The force generated is about proportional to the size of the enabler. This model can be applied to ProTeqt's current USB lock design, which uses the full size enabler directly on the surface of the deactivation tablet.

However, when deactivation is performed at one-inch distance, the half-size enabler has better performance with 90% confidence. As explained in Chapter 4.2, larger size enabler has more damping effect on the LC circuit resulting a worse coupling.

Table 4 Force test result of full-size and half-size enabler

		Mean	Std. Dev.
On tablet	**Full**	$11.1N$	$1.88N$
	Half	$4.45N$	$1.16N$
1 in. above	**Full**	$4.12N$	$1.10N$
	Half	$6.56N$	$1.11N$

Based on the experimental results shown, we learned that there is an optimal enabler size. When enabler is small, the size effect is dominant, and therefore larger enabler is better. When enabler is large, the damping effect becomes dominant, and therefore smaller size is better. Limited by the time constraint, the size of enabler was not optimized during the project. For system scale analysis of the Micro-USB lock, the half-size enabler was used thanks to its superior performance to the full-size enabler.

5.3 Force Test Results

5.3.1 Mechanical Lock Force

The analytical model gives force of 7 and 20N for the respective frictional and bending forces. The total force required using this analysis is 27N. After stepping through several iterations of the FEA using different forces, we found that a force of 15N would give a reasonable amount of displacement. In contrary, the force data collected resulted with a mean of only 1.844N with a standard deviation of 0.3048N. This is significantly lower than the either of the two previous force analyses.

The analysis assumes that the two sheet metal pieces have zero deviation from their dimensions. That is, the components mesh together in a perfect manner. Realistically, the clearance between parts in the y-axis can significantly reduce the amount of force required to disengage the two sheet metal components. For the calculation of frictional force, the assumption is that the two surfaces that will be sliding past each other are perfectly parallel, making solid contact. In reality, the components are very small, and prone to burrs, inherent in stamped parts. The burrs provide and even smaller interface between the two components, which would lessen the frictional force. Because of the assumptions made, the calculations and FEA model can be used as a tool to understand the extreme maximum values for both the frictional and bending forces, but they cannot show the actual force needed.

5.3.2 Force Generated by Enabler

The force generated by enabler is shown in Table 4. The half-size enabler can generate mean force of 6.56N at one-inch distance, which is significantly larger than the 1.844N

force needed to disengage the lock. If we assume that the measured data are normally distributed, and put the distribution of the two forces on one probability plot (Figure 25), it is obvious that the probability of enabler force smaller than required force is negligible. In other words, the chance of failure for this locking mechanism is very small. Detailed statistical analysis about the failure rate can be found in Krogman's thesis [21].

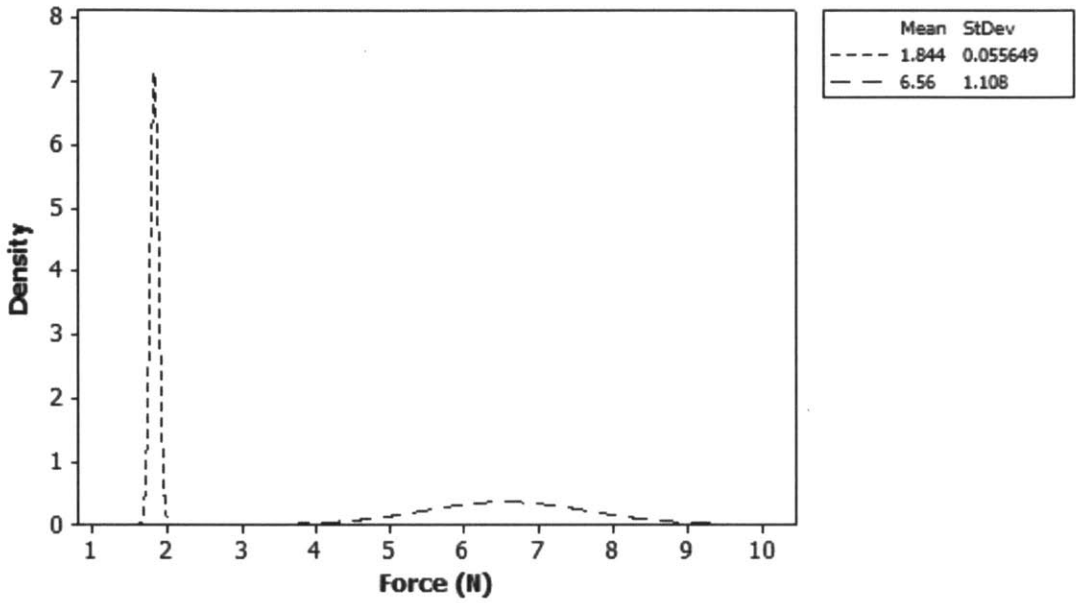

Figure 25 Force distribution. Small dash: disengagement force. Large dash: half sized enabler at 1" above the tablet.

6 System Performance Analysis

6.1 Objective

The objective is to provide ProTeqt with a tool, which can be used to predict the failure rate from a system standpoint. In addition, it will be helpful when defining the manufacturing quality control limit in the future. This section introduces a statistical method to assess the possibility of failure. The variability of the LC circuit due to manufacturing variation was measured via natural frequency (ω_n) using the sample coils and capacitors. Then, the relationship between the ω_n of a circuit with its corresponding efficiency at 220kHz and the relationship between efficiency and force generated by enabler at one-inch distance. With this information, the force generated by an enabler when paired to LC circuit can be predicted. Since the force needed to disengage the sheet metal lock is known from the force analysis in Chapter 5, the failure rate can then be evaluated. Due to the lack of data, a simulation model was developed to generate data, and help process the calculation.

6.2 LC Circuit Variation

LC Circuit design and optimization for the application at 1 inch uses an assumption that each LC circuit manufactured will be made to the nominal natural frequency. However, due to the inherent variability found in manufacturing processes, the actual natural frequency will vary. To have a better perspective on the performance of the circuit when manufactured at volume, we can obtain variance estimation for the inductor and capacitor. Using these values we can calculate any variation associated with the manufacturing of the circuit, and therefore complete an analysis of the frequency distribution based upon the process variation of the LC circuit.

6.2.1 Data Collection

The process of determining variation in the LC circuit began by randomly selecting 10 coils of each type that were produced by a contract manufacturer. Each type of coil was produced to the same specification, using techniques that mimic large-scale production.

In total, there were 6 types of coils with same inner diameter, but various gage sizes and number of turns. The variation of the coil is measure by inductance at 1kHz and 0.2V using an LCR meter. Measuring at different frequency or voltage will give different inductance value, but the overall distribution should not be different. The data was first compared between different types of coil to analyze the variation between groups. Then, all the data was pulled together and normalized to form the overall inductance distribution.

The test result of inductance shows that the coil winding process is well controlled. The coefficients of variation (CV)[4] are all below 3%, and most of them are well below 1%. Detailed data can be found in Appendix B. The manufacturing variation of the capacitor is also promising. With mean of 0.96μH and standard deviation of 0.0045, the CV of the 16 sample capacitors is only 0.47%. This very low variation contrasts with the manufacturer specification of 20%. After consulting the capacitor manufacturer, we were told that variation from batch to batch does exist, and they could not guarantee that the variation will always be similar to what we observed. To be conservative, we will rely on the specification and assume that the tolerance given is six standard deviations, or an effective CV of 3%. [Note: If 6 sigma/mean = 20%, then CV = 1 sigma/mean, so we get 20%/6 ≈ 3%.]

Fifteen circuits were assembled to measure natural frequency with the half-size enabler at one-inch distance. The mean natural frequency is 218kHz, which is close to the optimal 220kHz. The CV of natural frequency was calculated at 3.70%, which is higher than the one of inductance and capacitance owing to the stack-up variation of inductance and capacitance. Detailed data is exhibited in Appendix C.

6.3 Relating Efficiency to Natural Frequency

The efficiency of a magnetically coupled circuit is defined by Eq. (4.2). Based on experiment, we found that the shape of the efficiency curve of an LC circuit is independent of its natural frequency, but the peak of the curve does shift with natural

[4] CV is defined as the ratio of the standard deviation to the mean of a random variable

frequency. As shown in Figure 26, the two LC circuit with natural frequency 5% below and 15% above 220KHz have similar efficiency curves as the one of the 220KHz circuit. Thanks to this character, if the natural frequency of an LC circuit is known, its efficiency on the deactivator is predictable without any testing. The efficiency of any circuit at 220kHz $\{Eff_{220}(f_0)\}$ can be obtained using a translation of the efficiency plot of a 220kHz circuit $\{Eff(f_0)\}$. The transition can be expressed as:

$$Eff_{220}(f_0) = Eff(220\ kHz - (f_0 - 220\ kHz)) \tag{6.1}$$

where f_0 is the natural frequency of a circuit.

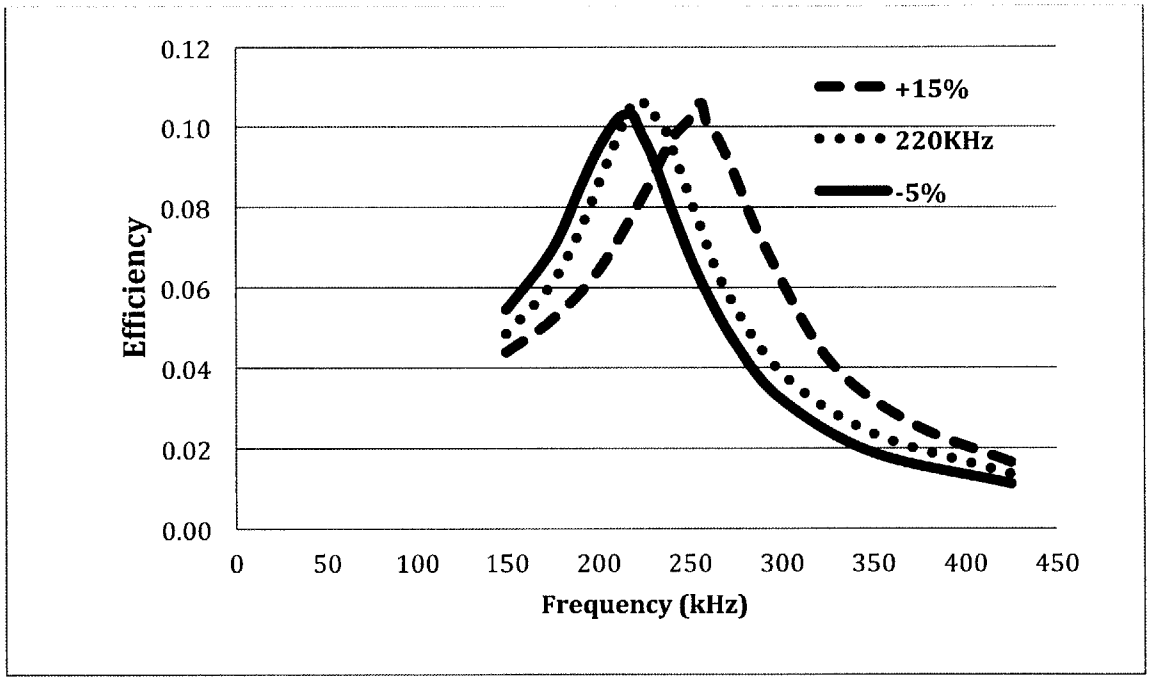

Figure 26 Comparison of efficiency plots at three different resonant frequencies: 220 kHz, 210 kHz (-5%) and 250 kHz (+15%)

A non-linear regression model converting natural frequency to efficiency was fitted using the following function:

$$Eff_{220} = \frac{1}{\theta_1 + \theta_2(f_0 - \theta_3)^2} \tag{6.2}$$

where $\boldsymbol{\theta_1, \theta_2, \theta_3}$ are constant.

This model assumes that the curve is symmetric about the peak ($\boldsymbol{\theta_3}$). It is true in theory, and based on the efficiency plot, the assumption is valid. For this project the peak frequency is set to 220kHz.

With mean square error of only 2.01e-5, the regression model obtained with Minitab is a good representation of the data. The summary of the model is listed in Table 5. The fitted line plot and the regression model are shown in Figure 27.

Table 5 Efficiency vs. Frequency Regression Model Summaries

Holiday Regression	
$\boldsymbol{\theta_1}$	9.70087
$\boldsymbol{\theta_2}$	$2.73731\times10^{-9}Hz^{-2}$
$\boldsymbol{\theta_3}$ **(fixed)**	220,000 Hz
Degrees of Freedom	14
Mean Square Error	2.01×10^{-5}

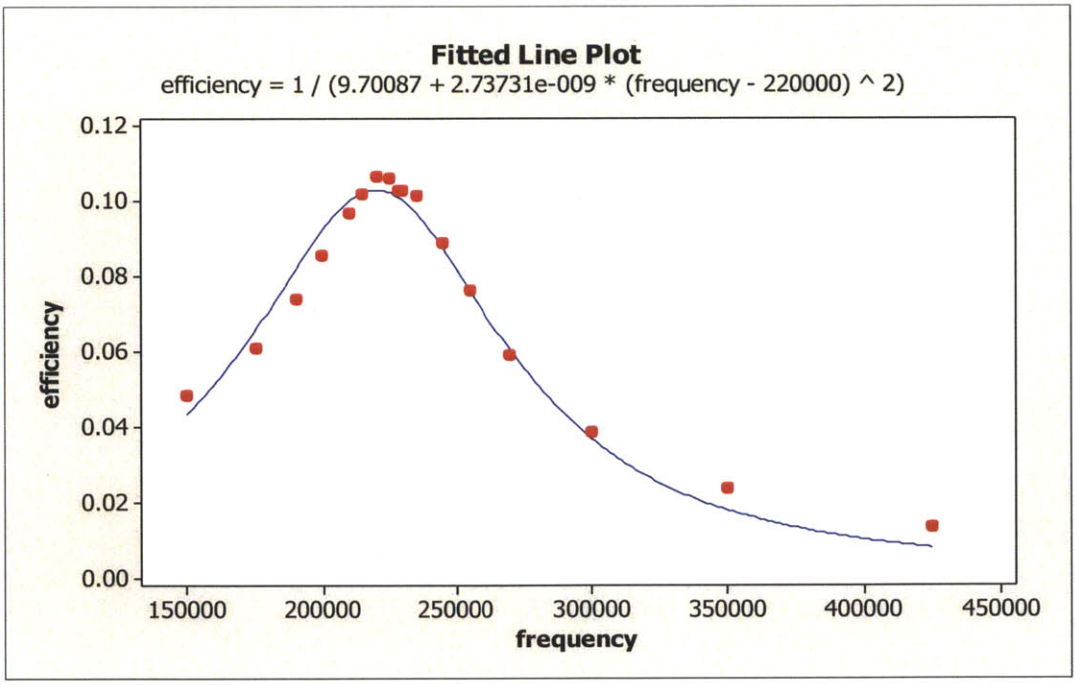

Figure 27 Plot of Regression Model Fit

6.3.1 Probability Distribution of the Force Generated by Enabler

The force generated by the enabler varies depending on the natural frequency of the LC circuit and the property of the enabler such as the size and the uniformity of the epoxy in the enabler. Three coils with natural frequency of 220kHz, 15% higher than 220kHz and 5% lower than 220kHz were made to represent the variability of the LC circuit. Ideally, the size, uniformity and other parameter of the enabler should also be set as controlled effects to test the output. However, limited by the resources we had, none of the effects could be quantitatively controlled. Therefore, the error caused by enabler's variation to the output was combined with measurement error.

The deactivator was designed to run at 220kHz. Based on the test result from previous section, on the deactivator the coil with natural frequency of 220kHz had the highest efficiency, which in theory means that it should have the best performance. In order to understand how the efficiency figure corresponding to the actual force generated from the enabler, an experiment need to be performed.

The experiment is identical to the one used for the enabler force test. According to the test result from the enabler force analysis, a half-size enabler in general has better performance at one-inch distance [20]. For this reason, the focus will be only put on the half-size enabler. Each of the three coils will be used to activate 10 half-size enablers. The force generated will be recorded, and the mean will be used as the corresponding force of each coil. The three data points of the mean force will be enough for us to fit a regression model of force with respect to natural frequency. Since the efficiency plot is about symmetric about 220kHz, and the force should be positively corresponding to the efficiency, we are expecting to see the force plot to have a similar shape as the efficiency plot.

6.3.2 Quality Control Limit

Combining the force plot with the natural frequency distribution, the distribution of the force generated by the enabler (F_{gen}) can be created. The distribution of the force required to open the lock (F_{lock}) was developed through the mechanical lock force analysis. If we take the difference between these two random variables, we can obtain a

new random variable $Y = F_{gen} - F_{lock}$, with mean of $\bar{Y} = (\bar{F}_{gen} - \bar{F}_{lock})$ and variance of $\sigma_Y^2 = \sigma_{F,gen}^2 + \sigma_{F,lock}^2$. The failure rate due to the variability of all the components is the probability of $Y \leq 0$. For the same lock design, using components with smaller manufacturing variability will reduce deviation of F_{gen}, and therefore reduce probability of failure. In order to achieve the target failure rate, the quality control limit can be calculated backwards using the model we obtained.

6.4 Simulation Model

In order to process the calculation needed such as combining two distributions, a simulation model is needed. It can also be used to generate critical data, which were not able to be collected during the span of this project. Taking both the data measured and simulated, the simulation model can stack up the variations in the whole system, and output the failure rate. The result can help us to access the robustness of the current design. In addition, a sensitivity test was performed to demonstrate how this program could be used to choose the capacitor with proper accuracy (typically 5%, 10% or 20%).

6.4.1 Assumptions

Based on the measurement data collected (Appendix C), we assumed that the distribution of inductance L and capacitance C were normal. In the model, the value of inductance and capacitance were generated using the mean (μ_L, μ_C) and standard deviation (σ_L, σ_C) measured from samples. The variation of the capacitance is based on the manufacturer specification of 20%. We assume that $\pm 20\%$ is equivalent to $\pm$six-sigma level.

The relationship between efficiency (Eff) and force generated by enabler (f_{gen}) could not be obtained owing to the lack of a working deactivator. In the simulation, we assumed a linear relationship between the efficiency and mean force, which can be represented as:

$$\bar{f}_{gen} = \bar{f}_{gen,max} \frac{Eff}{Eff_{max}} \tag{6.3}$$

As we observed from the result of force analysis, even with the same circuit, due to the inherent variation of the enabler, the force generated is random. In the model, for every circuit, we use the same CV obtained from force test data (half-size pillow, natural frequency at 220kHz) to calculate the standard deviation (σ_{gen}) of the force. Using the mean force and the standard deviation, we can generate normal distribution for f_{gen}.

6.4.2 Conditions

According to the result from coil design and force analysis, the lock design with best performance at one-inch distance is the one with AWG24, 9-turn coil, $1\mu F$ capacitor, and a half-size enabler [20]. The simulation was run based on this setup. In the coil design phase, we observed that with half-size enabler, the resonance frequency of an LC circuit is about 19kHz higher at one-inch distance than its natural frequency with no standoff. In the simulation, this shift is added to all the data points.

6.4.3 Inputs

The simulation program requires the following inputs listed in Table 5 to perform the calculation:

Table 6 Input Parameters for Simulation

μ_L	Mean Inductance	$0.63\mu H$
σ_L	Standard Deviation of Inductance	$0.00665\mu H$
μ_C	Mean Capacitance	$0.1\mu F$
σ_C	Standard Deviation of Capacitance	$0.033\mu F$
f_0	Natural Frequency of LC Circuit	
$\bar{f}_{gen,max}$	Mean Force Generated by the Optimal Circuit	$6.56N$

$\sigma_{f,gen}$	Standard Deviation of the Force Generated by the Enabler with the Optimal Circuit	1.108
$\bar{F}_{lock}$	Mean Force Needed to Disengage the Lock	1.844
$\sigma_{F,lock}$	Standard Deviation of the Force Needed to Disengage the Lock	0.3048

6.4.4 Operation

The program first took the sample mean and standard deviation to generate a normal distribution of inductance and capacitance with 100 data points each. Then the distribution of natural frequency was calculated by randomly combining an inductor with a capacitor. This operation generated the natural frequency of 100 coils. Each coil was assigned to a corresponding efficiency value based on the efficiency plot equation (Figure 27). Using the efficiency-force Equation (6.3) and $\sigma_{f,gen}$, the force distribution of each coil was obtained. The simulation program is able to sum up the force distribution associated with each coil, and calculate the overall force distribution (F_{gen}). Because the force distribution of each coil was assumed to be normal, the overall force distribution was expected to be normal as well. Ultimately, the program can calculate the probability of failure by comparing the two distributions of force generated and force required.

6.4.5 Output

Table 7 Summaries of the Output from Simulation

F_{gen}	Force Generated by the Enabler
$\sigma_{F,\ gen}$	Standard Deviation of Force Generated
P_{fail}	Failure Rate

6.4.6 System Sensitivity Analysis

This entire simulation was run three times, with three different levels of capacitance quality: 5%, 10% and 20%[5]. The objective of this test was to understand how the quality of capacitor would affect the performance of the system, more specifically the distribution of force generated.

6.5 Simulation Results

6.5.1 LC Circuit Variation

The distribution of Natural Frequency is well simulated by MATLAB. The data is normally distributed with Skewness of -0.0177 and Kurtosis of -0.488. As we can see in Figure 28, the natural frequency is normally distributed with mean around 220kHz.

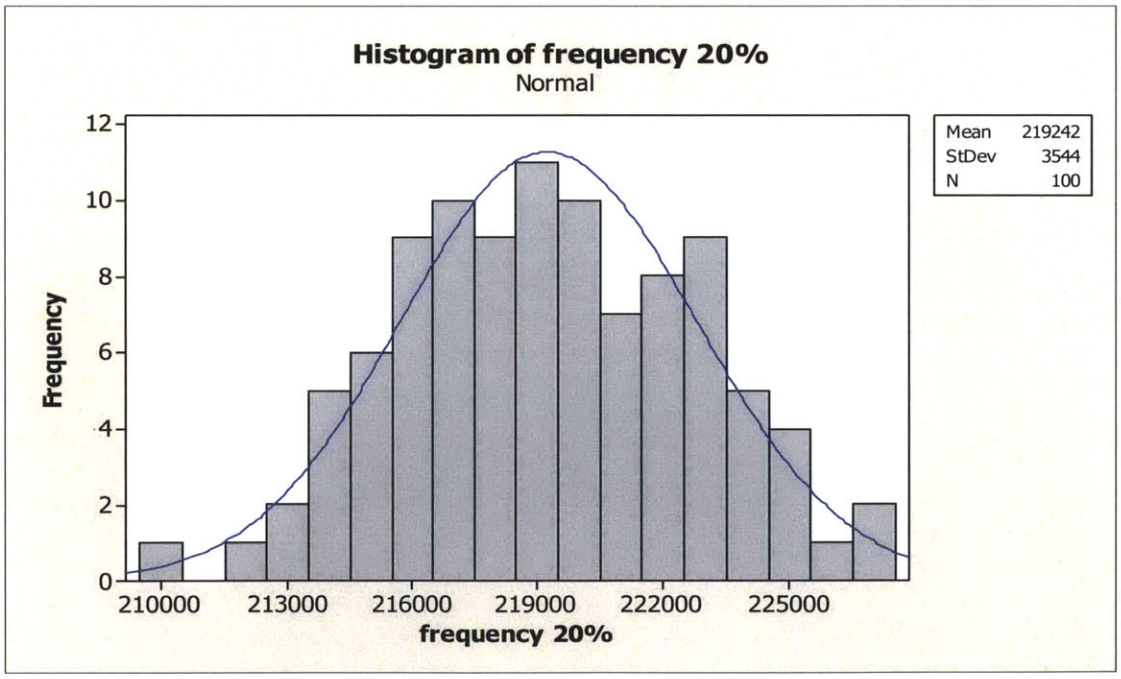

Figure 28 Histogram of Natural Frequency (20% Capacitor)

[5] Where this range is assumed to represent ±6 sigma

The distribution of efficiency, however, is not normally distributed. It is exactly how the distribution ought to be because circuits with either higher or lower natural frequency will have efficiency smaller than the peak efficiency. The histogram of efficiency (20% capacitor) is presented in Figure 29. The distribution has high density around maximum efficiency and a long tail toward the left end.

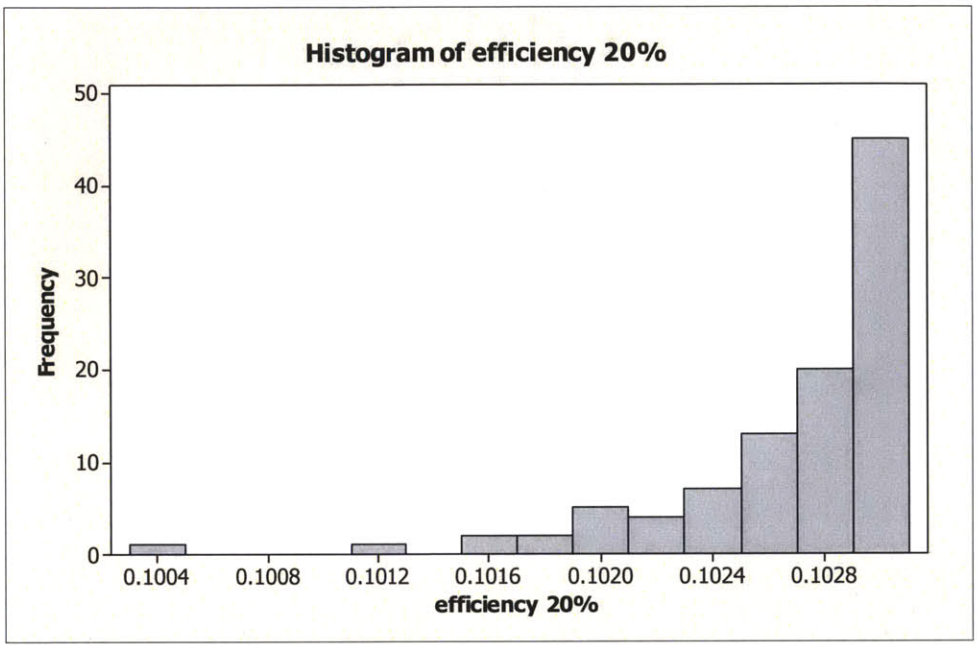

Figure 29 Histogram of Efficiency (20% Capacitor)

6.5.2 Force Distribution

The histogram of the force distribution (20% capacitor) presented in Figure 30 is normally distributed as expected.

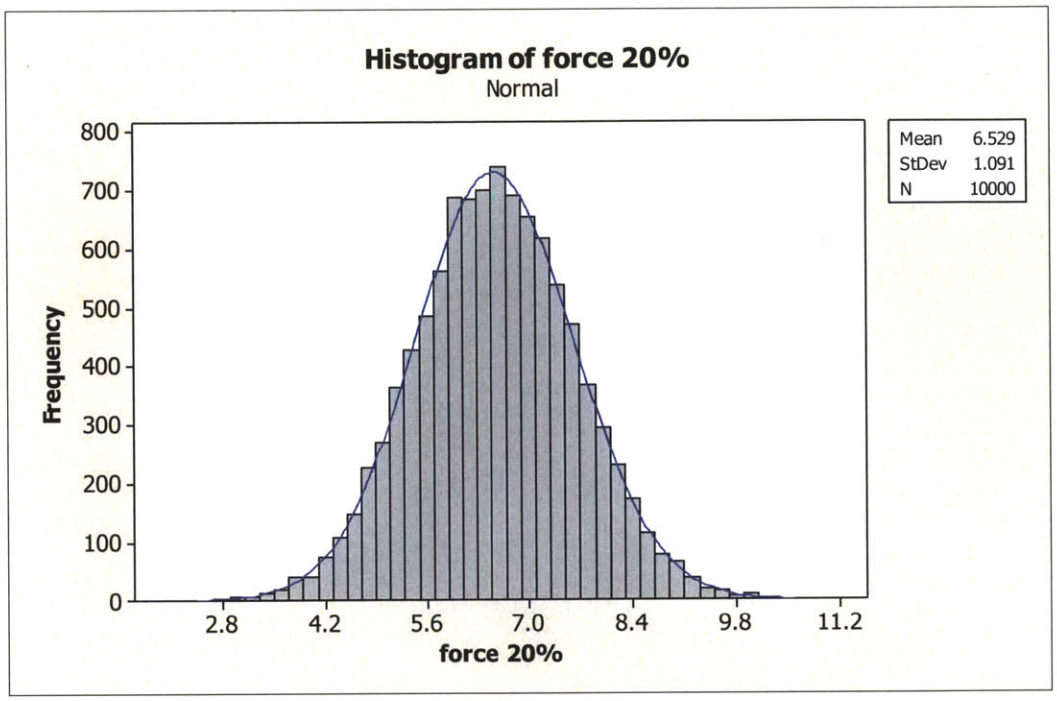

Figure 30 Histogram of the Force Generated by Half-size Enabler

The characteristics of the distribution are summarized in Table 8.

Table 8 Force Histogram Summaries

Mean	6.5295 *N*	**Skewness**	−0.0157
Standard Deviation	1.0909 *N*	**Kurtosis**	0.0101
95% C.I. for mean		[6.5081 ; 6.5509]	
95% C.I. for standard deviation		[1.0760 ; 1.1062]	

According to the simulation result, we found that the force generated by the enabler is significantly higher than the 1.844N force needed to disengage the lock even with the 20% capacitor.

6.5.3 System Sensitivity Analysis with Various Capacitors

As expected, the standard deviation of the frequency distribution increases as the capacitor quality decreases (Table 9). However, as shown in Table 10, the capacitor quality does not affect the standard deviation of the enabler force distribution as the 95% confidence intervals of all three standard deviations overlap. In the particular case of this realization, the estimate of the standard deviation for 20%-capacitor is even smaller than the 5% and 10%-capacitors. This phenomenon is ascribed to the rather large manufacturing variability of the enablers. Thus, the force distribution that can be generated has a significantly higher variance than the electrical components. From this simulation, it appears that the use of 20%-capacitor would not damage the performance of the lock. However, the manufacturing variability of the enabler should be kept under control. At the time of this thesis, the enabler was made by hand in small quantities (several thousands). Manufacturing control of this part was not a priority for ProTeqt yet.

Table 9: Resonant frequency distributions

Cap. Quality	5%	10%	20%
Mean	219,469 *Hz*	219,585 *Hz*	219,242 *Hz*
Standard Deviation	1,018 *Hz*	2,095 *Hz*	3,544 *Hz*
95% CI for mean	[219,266 ; 219,271]	[219,169 ; 220,000]	[218,782 ; 221,069]
95% CI for std. dev.	[894 ; 1,183]	[1,840 ; 2,434]	[3,112 ; 4,117]

Table 10: Force distributions

Cap. Quality	5%	10%	20%
Mean	6.5527 *N*	6.5497 *N*	6.5295 *N*
Standard Deviation	1.1005 *N*	1.1015 *N*	1.0909 *N*
95% CI for mean	[6.5311 ; 6.5743]	[6.5281 ; 6.5713]	[6.5081 ; 6.5509]
95% CI for std. dev.	[1.0854 ; 1.1159]	[1.0864 ; 1.1170]	[1.0760 ; 1.1062]

Because assumptions such as a linear relationship between efficiency and force were made in the simulation model due to the lack of data, getting a quantitative failure rate or a quality control limit is not meaningful. The simulation model qualitatively draws the conclusion that the lock system is very robust. Based on the actual testing we performed with the lock, we did experience a high rate of success when disengaging the lock, which is coinciding with the simulation result.

7 Conclusion and Future Work

7.1 Conclusion

By the end of this project, we have proved that the solution of adding a resonantly coupled LC circuit to the system will enable the lock to be deactivated at the distance of one inch above the deactivation tablet. Working in the field of deactivation at distance, we have drawn other conclusions.

7.1.1 LC circuit design

Given the existing design of the lock, the most effective wound coil is a 9-turn coil with a wire gage of 0.5mm (AWG 24). In addition, we recommend decreasing the size of current enabler (9mm by 12mm) to increase the loss of coupling efficiency due to the enabler. Based on our tests, using a rectangular piece of 9mm by 6mm provides much better results.

For more general considerations:

- The loss of coupling efficiency is largely determined by the ratio of the enabler size over the coil size. We recommend keeping the enabler smaller than the coil.
- In order to optimize the design of the circuit, one must primarily maximize the induced current through it.
- Up to a certain point that is not studied in this thesis, an efficient coil has a large gage size and a high number of turns.

A coil winding process should be used to manufacture the inductor component of the circuit, as it is a well-established process that can produce quality coils at a very low price. If other manufacturing techniques are considered, a design change may be necessary for the coil, especially if the thickness of the conductive material is small (printing, etching, etc.). In this case, we recommend considering the design proposed on Appendix A. In this design, the coil consists of several parallel lines. This design

decreases the resistance of the coil without sacrifice inductance. However, the exact design has not been optimized yet (number of parallel lines, number of turns, thickness, etc.). The design will also depend on the manufacturing method.

7.1.2 Lock Mechanism

At one inch above the deactivator, half-sized enabler (9mm x 6mm) can generate more force than the full-sized enabler (12mm x 9mm), providing more reliable deactivation results. Thus, the smaller enabler is recommended for this application. On average, the lock requires 1.8N force to disengage, which is significantly less than the average 6.56N a half-sized enabler can generate. As the result, the deactivation process has very low failure rate. Now, it is crucial to have a more reliable tablet.

7.1.3 Effect of LC Circuit Variability on Lock Reliability

Due to the availability of the deactivation tablet, several crucial tests could not be performed to obtain quantitative analysis about the overall force distribution of enabler. A numerical simulation with strong assumptions was implemented to create the distribution. At the end, it appears that the quality of the capacitance does not significantly affect the performance of the lock. The use of 20%-capacitance should be sufficient for this application. Instead, the simulation exhibits the predominance of the enabler manufacturing variability. Currently, enablers are made by hand in small batches. If this method is pursued for full-scale production, it is recommended that the process is performed with the help of machinery to ensure consistency.

7.2 Future Work

7.2.1 Micro-USB Lock

In regards to the LC circuit design, other manufacturing methods could be considered, such as etching or inkjet printing. This thesis proposes the alternative design (Appendix A), but it is not totally defined, and substantial future research is required.

More data are required to accurately evaluate the failure rate of the lock at deactivation, especially at one inch above the tablet. The relationship between efficiency and force generated (Eq. 6.3) was assumed to be linear. More force tests needs to be done with circuits that have various natural frequency.

Finally, we find that the size of the enabler is important in terms of lock reliability and should be optimized. The shape of the enabler may also be a critical parameter. Some preliminary experiments conducted at ProTeqt show that the corner of the rectangular shaped enabler might be redundant thermal mass. Thus, further investigation should be done on other shapes, especially circular. In addition, the conductive material laminated on the enabler for heat generation need further study as well. The thickness and the material used are both significant parameters.

7.3 Theft Denial System

The current generation theft denial system transfers strong energy wirelessly to the lock via radiofrequency for deactivation. It requires a robust design of the deactivation tablet to handle the intense power. More work is needed to develop a reliable tablet. The radiofrequency intensity degrades significantly with distance. To achieve deactivation distance of more than one inch, ProTeqt has to develop either a tablet with higher power output, or a method that can transfer power more efficiently.

At present, the retail industry is seeking for a completely new experience at the point-of-sale. Thanks to the progress of non-contact technology, it will be possible to checkout the products without physical touch. It is worthwhile for ProTeqt to take a completely different approach that uses weak signal instead of intense energy transfer for deactivation. An active lock with energy storage, such as battery, might be able to achieve this task. Thus, the next distance objective of ProTeqt might be several feet instead of one inch only.

8 References

[1] Finklea K., 2011, Organized Retail Crime, Congressional Research Service.

[2] Centre for Retail Research, 2011, "Centre for Retail Research, Nottingham UK," The First Worldwide Shrinkage Survey.

[3] Lee Y. L., and Sorrells P., 2004, MicroID 125 kHz RFID System Design Guide.

[4] Finkenzeller K., 2003, RFID Handbook: Fundamentals and Applications in Contactless Smart Cards and Identification, John Wiley & Sons, Inc.

[5] Zahn M., 1987, RES.6-002 Electromagnetic Field Theory: A Problem Solving Approach, Spring 2008. (Massachusetts Institute of Technology: MIT OpenCourseWare), License: Creative Commons BY-NC-SA.

[6] Schauber M. J., Newman S. A., Goodman L. R., Suzuki I. S., and Suzuki M., 2007, "Measurement of mutual inductance from frequency dependence of impedance of AC coupled circuits using a digital dual-phase lock-in amplifier E ~ Lock-in ampliier," American Journal of Physics, **76**(2).

[7] Tesla N., 1900, "Apparatus for Transmission of Electrical Energy."

[8] Kurs A., Karalis A., Moffatt R., Joannopoulos J. D., Fisher P., and Soljacic M., 2007, "Wireless power transfer via strongly coupled magnetic resonances.," Science (New York, N.Y.), **317**(5834), pp. 83–6.

[9] Karalis A., Kurs A. B., Moffatt R., Joannopoulos J. D., Fisher P. H., and Soljacic M., 2009, "Wireless energy transfer," US Patent 8097983, **2009**, pp. 1045–8.

[10] Georgakopoulos S. V., and Jonah O., 2011, "Optimized wireless power transfer to RFID sensors via magnetic resonance," 2011 IEEE International Symposium on Antennas and Propagation (APSURSI), pp. 1421–1424.

[11] Cannon B., and Hoburg J., 2009, "Magnetic resonant coupling as a potential means for wireless power transfer to multiple small receivers," IEEE Transactions on Power Electronics, **24**(7), pp. 1819–1825.

[12] Beckwith L., 2013, "Inductor Theory," General Linear Systems.

[13] Lee Y., 1998, RFID Coil Design.

[14] Universe P., 2013, "Printed circuit boards," PCB Universe [Online]. Available: http://www.google.com/patents?hl=en&lr=&vid=USPAT4751146&id=9lIyAAAA

EBAJ&oi=fnd&dq=Printed+Circuit+Boards&printsec=abstract. [Accessed: 27-Jul-2013].

[15] SAWYER A., 2010, "Fabrication of nanofluidic devices using electrochemical etching of sacrificial copper."

[16] 2013, "Red C12000 Oxygen Free Copper Wire" [Online]. Available: http://www.alibaba.com/product-gs/430200636/Red_C12000_Oxygen_Free_Copper_Wire.html.

[17] Numakura D., 2008, "Advanced Screen Printing 'Practical Approaches for Printable and Flexible Electronics'," 2008 3rd International Microsystems Packaging Assembly Circuits Technology Conference, pp. 205–208.

[18] Hoban M., and Lunt B., 1997, "Soldering," The Technology Interface, **26**(5) [Online]. Available: http://www.ncbi.nlm.nih.gov/pubmed/23822908.

[19] Salmeron J. F., Torres A. R., Banqueri J., Carvajal M. a., and Agudo M., 2012, "Design and Characterization of Ink-Jet and Screen Printed HF RFID Antennas," 2012 Fourth International EURASIP Workshop on RFID Technology, pp. 119–123.

[20] Rony A., 2013, "Analysis and Design of Resonant Inductively Coupled Circuits: Application to Benefit Denial Solutions for the Retail Industry," Massachusetts Institute of Technology.

[21] Krogman M., 2013, "Design and Manufacturing Analysis of Resonantly Coupled Circuits and Other Components used for Applied Wireless Power Transmission: Application Analysis."

Appendix A: The Case of Thin Wire Coil

All the previous analysis has been conducted with winding copper coils. They are indeed easy to make in small quantity and very flexible. However, we may want to consider other manufacturing methods for full-size production, especially etching or inkjet. Beside their costs, with these methods, only coil with a very thin copper layer can be produce. As a consequence, their resistance will be significantly higher). In this application, efficiency of a coil is measured by the intensity of current that can be induced. Thus, it is important to achieve low resistance. So, the actual optimized design has to be reviewed for the case of thin wires.

In order to decrease the resistance of the coil, we propose a new design, inspired by the litz-wire solution. The printed coil consists of three parallel lines in spiral (see Figure 31 right). In order to get a coil with the same size as the regular design, the new design has only three full turns.

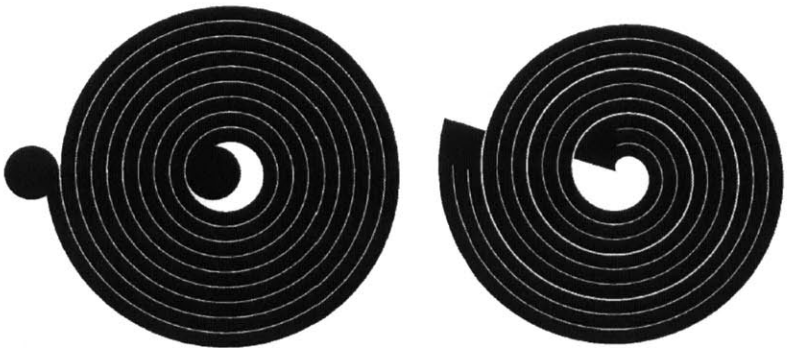

Figure 31: Regular coil design (left) and thin wire coil design (right)

This design is expected to significantly decrease the resistance of the coil. However, further tests have to be conducted to verify if this design effectively increases the magnitude of the secondary magnetic field.

Appendix B: Coil Inventory from Manufacturer

	1	2	3	4	5	6
Layer	one	two	one	three	one	one
OD in (mm)	0.35*0.47 (8.9*12)	0.35*0.47 (8.9*12)	0.35*0.47 (8.9*12)	0.35*0.47 (8.9*12)	0.35*0.47 (8.9*12)	0.35*0.47 (8.9*12)
Wire Gauge	ϕ0.32mm	ϕ0.32mm	ϕ0.5mm	ϕ0.2mm	ϕ0.5mm	ϕ0.2mm
Number of turns	9	16	6	47	9	9
Inductance (μH) 1KHZ 0.25V	0.61	1.7	0.25	14.25	0.63	0.61
STDEV of Inductance from Samples	0.00665	0.00326	0.00264	0.01984	0.01888	0.00679
Resistance (mΩ)	46.1	79.1	13.4	586	23.7	96

Appendix C: Natural Frequency Variability Measurement Data

Natural Frequency of sample LC circuits	*f* - Directly Driven (@RT)	f, 1.0", half enabler
1	200900	205000
2	219900	224000
3	214000	223100
4	216000	225600
5	218700	209800
6	219000	227900
7	216900	225900
8	214500	221900
9	220000	228400
10	219500	228300
11	206300	214500
12	204400	211000
13	205000	212500
14	204300	210500
15	207300	212600
Mean	212446.6667	218733.3333
Std	6905.780877	8083.19833

Appendix D: Matlab Code

```
n1 = 100; % sample size of frequency
f_tab = 220E3; %tablet frequency
%----- frequency ----------------------------------------------------------
muL = 0.63E-6; sigL = 0.008828905*muL; % inductance
muC = 1E-6; q = 0.2; sigC = q*muC/6; %capacitance; q is the quality
shift = 19E3; % frequency shift due to the enabler
L = muL + sigL.*randn(n1,1);
C = muC + sigC.*randn(n1,1);
f = shift + 1./(2*3.14.*sqrt(L.*C));
xlswrite('freqPDF.xlsx', L, 'MatlabExport', 'K2');
xlswrite('freqPDF.xlsx', C, 'MatlabExport', 'L2');
xlswrite('freqPDF.xlsx', f, 'MatlabExport', 'M2');
%----- efficiency ---------------------------------------------------------
theta1 = 9.70087; theta2 = 2.73731E-9; theta3 = f_tab;
eff = 1./(theta1 + theta2.*(f-theta3).^2);
xlswrite('freqPDF.xlsx', eff, 'MatlabExport', 'N2');
%----- force --------------------------------------------------------------
% linear
n2 = 100; % sample size of force
eff_max = 1/theta1; Fmean_max = 6.56;
Fdev_max = 1.108; cv = Fdev_max/Fmean_max;
F = zeros(n1*n2,1);
A = randn(n2,1);
for i = 1:n1;
    Fmean = Fmean_max*eff(i)*theta1;
    F((n2*(i-1)+1):i*n2) = Fmean*(1 + cv.*A);
end;
xlswrite('freqPDF.xlsx', F , 'MatlabExport', 'O2');
```